DESIGN AND ANALYSIS OF NON-UNIFORM MIMO ARRAY FOR INTERFERENCE SUPPRESSION AND AUTOMOTIVE APPLICATIONS

MUHAMMAD OMER ZAREEN

DESIGN AND ANALYSIS OF NON-UNIFORM MIMO ARRAY FOR INTERFERENCE SUPPRESSION AND AUTOMOTIVE APPLICATIONS

by

MUHAMMAD OMER ZAREEN

in partial fulfillment of the requirements for the degree of

Master of Science

in Electrical Engineering

at Delft University of Technology,

to be defend publically on Friday August 31, 2018 at 09:30 AM

Thesis Committee:

Prof. dr. A. Yarovoy,	TU Delft
Dr. Faruk Uysal,	TU Delft
Prof. dr. ir. G. Leus,	TU Delft

CONTENTS

ABSTRACT

Automotive radars play a very important role in reduction of traffic accidents and casualties by making the vehicle fully self aware of its surroundings. For the vehicle to be fully self aware multiple sensors or radars have to placed in close proximity of each other on the body of the automobile. This will lead to interference between the radars which results in sub optimal performance of the radar system. Currently most of interference mitigation techniques employ various methods of signal coding algorithms, by assigning each radar a different code or modifying beamforming and angle of arrival algorithms to suppress the interference. Most of theses technique use and exploit the properties of the transmitted signal (signal processing techniques) for mitigating the interference. In this thesis the avenue of antenna array design for mitigation of interference is explored. By modifying the radiation pattern of the array, the antenna array will act as spatial filter against the incoming interference signals. In this thesis two techniques for designing the antenna array with improved radiation pattern are proposed. The design techniques are used to optimize the MIMO virtual array of the radar for low sidelobes and increased aperture, and the optimized virtual array is then factorized to obtain the Tx and Rx arrays. 2 virtual arrays of 12 elements and 24 elements are optimized using the design techniques. The performance of the various designs is ranked based on the output SINR of an adaptive beamformer. The simulations results show that the optimized MIMO arrays result in an improvement of up to 3.5dB in SINR in comparison to the currently used topologies. Finally, a prototype of the improved MIMO antenna system is modelled in CST MS design environment, and the superior performance of the designed array topologies over the existing array topologies is verified.

1

INTRODUCTION

1.1. CONTEXT

Radar technology has been with us since Christian Huelsmeyer demonstrated that radio waves can be used to detect the presence of distant metallic objects by detecting a ship in dense fog and later estimating the distance of the ship from the transmitter, for which he was awarded a patent in 1904, the idea of transmitting a signal and receiving its copy after some interaction with an object is rather intriguing. The major developments to the radar technology were made during the second world war. At that time radars were mainly used for air defence and military purposes, for example long range air surveillance and short range for detection of low flying objects. After the war , research and development continued on radar both for civilian and military use. One of the major developments in radar in civilian sector is the weather radar both on ground and in a passenger aircraft. Pilots can see the cloud formations, the state and severity of the weather that they cannot estimate using just visual information and can divert the plane's flight path to avoid severe weather. Along with weather radar, radars can also be used for imaging. Synthetic aperture radar (SAR) is a radar that can create 2d and 3d images of object by moving the radar over a specified area, by moving the radar, the aperture of the radar antenna is increased, resulting in high spatial resolution compared to the conventional beam scanning radars.

Lately, radars have started to make their way into the automotive industry. The application of radars in automobiles range from parking assistance, adaptive cruise control to self-driving cars. Radars in automobiles are being used as the primary sensors for detection of obstacles, pedestrians or other automobiles in the vicinity of the car. Considering the applications of radars in automobiles and growing interest of researchers and investors for these applications, one can say that autonomous driving is the future of the automotive industry, where the driver can complete other tasks or relax after a hectic day instead of focusing and spending more energy in driving.

1

1.2. MOTIVATION

To be truly effective for autonomous driving, the radar should be able to detect and distinguish between different targets in the vicinity of the car with high precision and take measures accordingly. A 360 degree coverage is required to precisely map the surroundings of the automobile and for that purpose multiple radar sensors have to be employed as seen in figure 1.1. For all the systems, the automotive radar sensors will detect and track obstacles, then automatically adjust the vehicle's orientation relative to the obstacle. In addition the sensors may issue a warning to the driver of an imminent collision and apply emergency braking.

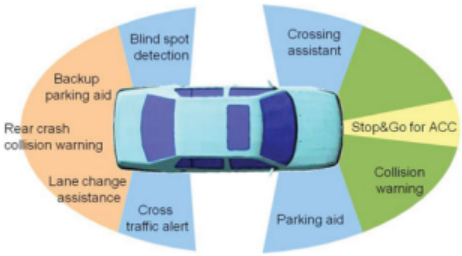

Figure 1.1: Automotive Radar Applications [1]

With all the different radars working at the same frequency and in close proximity to each other, interference is unavoidable. The interference between the radars and interference caused by surrounding autonomous vehicles can cause false alarms, miss detections and errors in measuring the range or the velocity of the target. After being detected, the interference can be mitigated either in spatial domain (by means antenna array and beam forming) or in time and frequency domains (by means of signal processing). In the recent years the main focus on automotive radar interference mitigation was on signal processing tools [2] [3] [4], while spatial filtering by means of radar antenna pattern forming has received little attention.

As a result, this project is focused on using the antenna array of an automotive radar as a spatial filter by modifying the radiation patterns of the Tx and Rx arrays in such a way that minimum power is received from the direction of the interference, coupled with signal processing algorithms to further reduce the effect of interference signals on the final radar output. By using the antenna as a spatial filter, simple processing algorithms can be used, which will reduce the computational complexity, time and power hence reducing the thermal noise of the receiver.

1.3. MIMO RADAR

Multiple input multiple output (MIMO) radars have been an important research topic for many researchers since it was introduced in [5]. Unlike traditional array radars, MIMO radar transmits different waveforms rather than scaled version of the same waveform with multiple antennas, in other words MIMO radars emit orthogonal waveforms rather than the same waveform which is focused using traditional transmitter-based beam-

forming [6],[7],[8]. The MIMO radar transmits omnidirectional orthogonal waveforms from each antenna element, therefore it illuminates all angles. The traditional radar system by using focused transmit beam has a higher processing gain then the MIMO system, but for some applications like scanning and imaging where all direction need to be illuminated at the same time, Tx beamforming is not efficient [6].

In MIMO receiver a matched filter bank is used to extract the orthogonal waveform components. There are two different approaches for using these noncoherent waveforms. In the first approach the transmitting elements are far enough from each other compared to the distance of the target from the radar, so the target RCS is different for different transmitted waveforms i.e. each orthogonal waveform will carry different information about the target, this will increase the spatial diversity and it can be used for better detection [6]. For the second approach the Tx elements are closer to each other than the distance of the target from the radar. Therefore, the target RCS is same for the orthogonal Tx waveforms. The phase difference caused by the different transmitting antennas along with the phased difference caused by the different receiving antennas can form a virtual array [6],[7],[9]. With a properly designed Tx and Rx antenna arrays one can from a large virtual array with small number of antennas, and the angular resolution of the radar can be increased dramatically.

1.4. INTERFERENCE AND METHODS OF SUPPRESSION

The interference can be coincidental. For example, if the target is another self-driving car the radar on that car will cause interference, at the same time interference can also be intentional. No matter the cause of interference, the effect of that interference is the same, it will degrade the quality of the signal at the receiving array of the radar, and a degraded signal will result in false detection, miss detections which in turn will cause accidents. As using a MIMO radar will increase the aperture of the receiving array of the radar by forming a virtual array, interference/jammer suppression capabilities of the radar will also improve. Most of the suppression techniques involve the use of adaptive beamformers, which create a null in the direction of the interference source i.e. they change the excitation amplitude and the phase of the signal at the antennas so that minimum power can be received from the direction of the interference source. But the number of interferes that can be suppressed is limited by the number of receiving array elements. The increased aperture of the MIMO radar will in turn increase the number of jammers that can be suppressed.

Even though the MIMO radar has high suppression capabilities, a 100 percent suppression is not possible. A large variety of methods to improve the performance of a MIMO radar exist, ranging from signal processing algorithms to boost the performance to antenna array design. In this thesis we will focus on the designing the Tx and Rx arrays of the MIMO system by having the goal of suppressing the interference and improving the performance of the MIMO system.

A large variety of antenna synthesis methods for achieving low sidelobes exists in the literature. Thinning the array has been a successful technique to achieve low sidelobes [10], by turning the elements of the receiver on and off to change the radiation pattern of the receiver array creating low sidelobes in the direction of the interference source. But for that purpose, switches at every antenna in the array are required to turn the an-

tenna on or off depending on the direction of the interference source. By minimizing the number of redundant spacing in the array the resolution and main lobe interference suppression capabilities of the MIMO radar can be improved [11],[12]. This will take away the need for switches at every element but at the same time will increase the computational complexity and time required to reach the final solution and may result in a Tx or Rx array too large to be physically manufactured.

Many evolutionary and generic algorithms have been used for designing aperiodic arrays with low sidelobes [13]-[16]. However, the complexity and the computational burden for these techniques increase with more number of elements. Particle swarm optimization is a high performance optimizer for array synthesis that is similar to the generic algorithms but requires less computational book keeping and generally fewer line of code [17]. To overcome the computational burden of the generic and other nature inspired design methods, deterministic synthesis techniques have been formulated [18]-[21]. Despite their higher computational performance and efficiency compared to the generic algorithms and other nature inspired design methods, the analytical complexity for these techniques is higher.

Synthesizing an array via convex optimization was first introduced in [22] as a computationally effective, easy to implement and an effective strategy to serve as an alternative to the existing design strategies. Many optimization methods have been purposed since then, including sparsity-based methods [23],[24] which can take into account the effect of mutual coupling [25], and optimizing the array for multiple beams [26] [27], and controlling the minimum spacing between elements [28] to avoid impractical inter-element separation in the final design.

Along with convex optimization, the method of polynomial factorization has also been used to design a sparse periodic linear array [29], factorizing the required effective aperture function to obtain the transmit and receive aperture function.

1.5. PROBLEM STATEMENT

Despite there being many algorithms and strategies to design an array with low sidelobes and lower First null beamwidth, none of the strategies have been employed in the synthesis of Tx and Rx arrays for a MIMO system. One of the reason is that the MIMO system not only depends on the Tx and Rx array but also the combination of the Tx and Rx arrays. If one was to optimize the arrays for a MIMO system he must optimize both Tx and Rx arrays, and even after that it is not a guarantee that the final MIMO pattern which is the product of the Rx and Tx arrays will be optimal for interference suppression.

The main goal of this research is use the avenue of antenna design in combination with signal processing techniques to increase the quality and performance of a MIMO radar. This work is divided into three parts:

1. Design a non-uniform Tx and Rx array for the MIMO system so that the virtual array is optimal for interference suppression.

2. Apply a suitable interference suppression algorithm (assuming the target and interference source positions are known) and rank the performance of the design strategies for the MIMO system. In this thesis the performance metric that will be used to decide the best topology will be the SINR (signal to interference plus noise

ratio) at the output of the adaptive beam former, as it will be an accurate representation of how effectively the final design works with the suppression algorithms.

3. Use CST MS design environment to model the Tx and Rx arrays and check the validity of the proposed design.

This report is divided into 6 chapters. Chapter 2 explains the MIMO signal model and derives a suitable beam former for interference suppression. Chapter 3 employs multiple design strategies, which include using thinning of the array to design a non-uniform Rx array for the MIMO system and using the method of convex optimization and polynomial factorization to design non-uniform Tx and Rx array for the MIMO system. Chapter 4 shows the final designs for the Tx and Rx arrays and ranks the performance of the final MIMO systems after suppression. Chapter 5 deals with the modelling of the single antenna and the radar with the Tx and Rx arrays and checks the viability if the proposed system using CST MS design environment. Chapter 6 gives the concluding remarks for the work and some recommendations for the future work.

2

MIMO Radar and Adaptive Beamformer

In this chapter we will discuss the operation of a MIMO system and derive an adaptive beamformer that will be used to suppress the signals incoming from interference sources present at different directions.

2.1. MIMO Radar

For a typical MIMO operation each transmit antenna emits a waveform independent of the other transmit antennas. There are two ways this can be achieved. Each transmit antenna will transmit the copy of the same signal but at different times similar to TDM (Time division multiplexing) or all the transmit antenna simultaneously radiate different waveforms that satisfy the orthogonality condition. Each receiving antenna will be able to receive these signals, as each transmit antenna is emitting different waveform, the echo signals at the receiver can be affiliated to each transmit antenna. From a transmit array of M elements and receive array of N elements, mathematically will result in a virtual array of MN elements with a larger aperture than the Rx array. The enlarged aperture will improve the spatial resolution and immunity to interference in comparison to a traditional radar.

2.1.1. MIMO Signal Model

Consider a radar system with M transmit antennas and N receive antennas. Both the Tx and Rx array are assumed to be close to each other. The *mth* element of the Tx array will emit the *mth* waveform of the Tx waveform vector $\phi(t) = [\phi_1, ..., \phi_m]^T$. The m transmit waveform satisfy the following orthogonality condition:

$$\int_T \phi(t)\phi^H(t)\,dt = I_M \tag{2.1}$$

Where, T is the pulse duration and I_M is the $M{\times}M$ identity matrix and $(.)^T$ and $(.)^H$ are the transpose and Hermitian transpose, respectively. The $N{\times}1$ receive vector at the

Rx array for each of the transmit waveforms can be written as:

$$\boldsymbol{x}(t) = \boldsymbol{x_t}(t) + \boldsymbol{x_i}(t) + \boldsymbol{n}(t) \tag{2.2}$$

Where $\boldsymbol{x_t}(t), \boldsymbol{x_i}(t)$ and $\boldsymbol{n}(t)$ are the target signal, interference/jamming signals and receiver noise respectively. The target signal can be written as:

$$\boldsymbol{x_t}(t) = \alpha_t(\boldsymbol{a}^T(\theta_t)\boldsymbol{\phi}(t))\boldsymbol{b}(\theta_t) \tag{2.3}$$

Where α_t is the complex valued signal from the target which is at an angle of θ_t from the radar, and $\boldsymbol{a}(\theta_t)$ and $\boldsymbol{b}(\theta_t)$ are the actual transmit and receive steering vectors given by:

$$\boldsymbol{a}(\theta_t) = [e^{j2\pi\frac{Pos_{tx_1}}{\lambda}\sin\theta_t}, e^{j2\pi\frac{Pos_{tx_2}}{\lambda}\sin\theta_t}, ..., e^{j2\pi\frac{Pos_{tx_m}}{\lambda}\sin\theta_t}] \tag{2.4}$$

$$\boldsymbol{b}(\theta_t) = [e^{j2\pi\frac{Pos_{rx_1}}{\lambda}\sin\theta_t}, e^{j2\pi\frac{Pos_{rx_2}}{\lambda}\sin\theta_t}, ..., e^{j2\pi\frac{Pos_{rx_n}}{\lambda}\sin\theta_t}] \tag{2.5}$$

Where Pos_{tx_m} and Pos_{rx_n} are the position of the *mth* transmit element and *nth* receiver array element with λ being the wavelength.

Assuming the target is observed in the background of J interference sources with a complex valued signal β_i for the *ith* interference source and at an angle of θ_i from the array, the *N×1* vector for interference sources at the receiver can be written as:

$$\boldsymbol{x}_i(t) = \sum_{i=1}^{J} \beta_i \boldsymbol{b}(\theta_i) \tag{2.6}$$

Where $\boldsymbol{b}(\theta_i)$ is the receive steering vector due to the interference source at θ_i. It can be given by:

$$\boldsymbol{b}(\theta_i) = [e^{j2\pi\frac{Pos_{rx_1}}{\lambda}\sin\theta_i}, e^{j2\pi\frac{Pos_{rx_2}}{\lambda}\sin\theta_i}, ..., e^{j2\pi\frac{Pos_{rx_n}}{\lambda}\sin\theta_i}] \tag{2.7}$$

At the receiver, the transmitted signal can be recovered by match filtering the received signal to each of the Tx waveforms:

$$\boldsymbol{x}_m(t) = \int_T \boldsymbol{x}(t)\phi_m^*(t)\,dt \tag{2.8}$$

where $m = 1.....M$.

By match filtering the received signal with M different waveforms, a *MN×1* virtual array data vector can be obtained. The MIMO virtual array data vector can be written as:

$$\boldsymbol{y} = [\boldsymbol{x}_1^T .....\boldsymbol{x}_M^T] = \alpha_t \boldsymbol{a}(\theta_t) \otimes \boldsymbol{b}(\theta_t) + \boldsymbol{y}_i + \boldsymbol{n} \tag{2.9}$$

The term $\boldsymbol{a}(\theta_t) \otimes \boldsymbol{b}(\theta_t)$ can defined as the steering vector of the virtual array, where $\otimes$ stands for Kronecker product of the steering vectors for transmitting and receiving array. Kronecker product can be defined as multiplication of the first element of the first vector with all the elements of the second vector, multiplication of the second element of the first vector with all the elements of the second vector and so on. The results of these multiplications are concatenated to from a single vector. So a Kronecker product of two

vectors with sizes *M×1* and *N×1* will result in a vector of size *M×(N×1)*. Thus the steering vector of the virtual array can be written as:

$$\boldsymbol{v}(\theta_t) = \boldsymbol{a}(\theta_t) \otimes \boldsymbol{b}(\theta_t) \tag{2.10}$$

$$\begin{aligned}\boldsymbol{v}(\theta_t) = [&e^{j2\pi \frac{Pos_{tx_1}+Pos_{rx_1}}{\lambda}\sin\theta_t}, e^{j2\pi \frac{Pos_{tx_1}+Pos_{rx_2}}{\lambda}\sin\theta_t}, ..., e^{j2\pi \frac{Pos_{tx_1}+Pos_{rx_n}}{\lambda}\sin\theta_t},\\ &, e^{j2\pi \frac{Pos_{tx_2}+Pos_{rx_1}}{\lambda}\sin\theta_t}, ...e^{j2\pi \frac{Pos_{tx_m}+Pos_{rx_n}}{\lambda}\sin\theta_t}]\end{aligned} \tag{2.11}$$

The vector $\boldsymbol{v}(\theta_t)$ comprises of phase shifts the waveform will experience from each transmitting antenna to each receiving antenna. The phase shifts in the virtual array steering vector can be used to find the angular position of the target. The target signal in equation 2.10 can be written as:

$$\boldsymbol{y}_t = \alpha_t \boldsymbol{v}(\theta_t) \tag{2.12}$$

The term $\boldsymbol{y}_i$ in equation 2.10 accounts for the interference signals in the virtual array, it can be expressed as:

$$\boldsymbol{y}_i(t) = \sum_{i=1}^{J} \beta_i \boldsymbol{v}(\theta_i) \tag{2.13}$$

Where, $\boldsymbol{v}(\theta_i) = \mathbf{1}_{\boldsymbol{M}} \otimes \boldsymbol{b}(\theta_t)$ is the *MN×1* virtual array steering vector for the interference source at θ_i. $\mathbf{1}_{\boldsymbol{M}}$ donates the *M×1* vector of all ones. The reason behind this is that the interference signals did not originate from the transmitting array of the MIMO radar, so the virtual array steering vector for the interference source will not depend on the transmit steering vector. The term $\boldsymbol{n}$ in equation 2.10 is the *MN×1* noise vector, for which the covariance matrix is defined as, $\boldsymbol{R}_n = \sigma_n^2 \boldsymbol{I}_{MN}$, where σ_n^2 is the noise power.

One of the main advantages of a MIMO radar over a conventional radar is the increased angular resolution. The minimum angular separation between two targets where the radar can distinguish the two targets is called the angular resolution of the radar. It depends on the beamwidth of the receiving antenna or array. Smaller the beamwidth better will be the angular resolution of the radar. The beamwidth of an antenna is inversely proportional to the antenna aperture, so by increasing the aperture of the receiving antenna or array, beamwidth will reduce hence increasing the angular resolution of the radar. As the MIMO radar allows us to increase the aperture of the receiving array, we can improve the angular resolution of the radar by using small number of physical antennas.

Various signal processing such as beamforming, Fourier transforms to obtain the range, speed and angle of arrival of the target, are applied on the virtual array data vector given in equation 2.10.

2.1.2. MIMO AUTOMOTIVE RADAR

MIMO system is the most preferred choice for an automotive radar, as small number of antennas can create a large array with higher angular resolution and interference rejection capabilities. As the automotive radars are set to operate at 24GHz and 77GHz bands, the antenna system for these radars fall in the class of mm-Wave antennas i.e. the size

of these antennas is very small, which is beneficial for an automotive radar as the space on an automobile is very limited, and using huge antenna systems is not practical. The small size of antennas coupled with a MIMO system gives a lot of freedom as in how many antennas can be used. For example if an antenna system of collocated 10 Tx antennas with spacing of $\lambda/2$ at 77GHz and 10 Rx antennas with spacing of $\lambda/2$ at 77GHz is used, a total of 17.53mm of space is required, in addition a virtual array of 100 elements with $\lambda/2$ spacing is created.

For this thesis, more practical designs of a MIMO automotive radar are considered. The 77GHz, 3 Tx and 4 Rx MIMO system developed by NXP Semiconductors is a prime example of such designs (Figure 2.1). By using just 7 collected antennas a virtual array of 12 elements can be created improving the angular resolution of the radar and at the same time less number of physical antennas will have less thermal noise and less computational power is needed for processing.

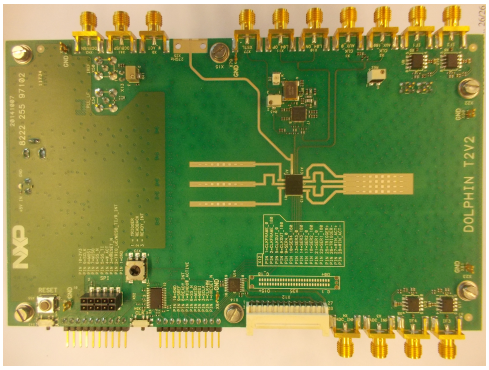

Figure 2.1: The NXP Automotive Radar System

The 3 Tx elements in figure 2.1 are spacing out by 2λ at 77GHz, while the spacing between the 4 Rx elements is $\lambda/2$ at 77GHz. Figures 2.2 shows the radiation patterns for the Tx and Rx arrays. The pattern of the virtual array also known as the Two-way pattern, is the product of the patterns of the Tx and Rx arrays. Keeping that in mind and looking at the radiation patterns for Tx and Rx arrays in figure 2.2, the 2λ spacing between the Tx elements and $\lambda/2$ spacing between the Rx elements makes sense, as the effective aperture of the Tx elements is equivalent to an array of 12 elements, making the main lobe width equal to that of an array of 12 elements (20°) and the nulls of the Rx elements are placed perfectly to cancel the grating lobes of the Tx array, thus creating a pattern similar to that of 12 elements with $\lambda/2$ spacing and a main lobe width of 20° and Side-lobe level of -13.07dB . Figure 2.3 shows the pattern of the virtual array formed for the 3 Tx and 4 Rx MIMO system.

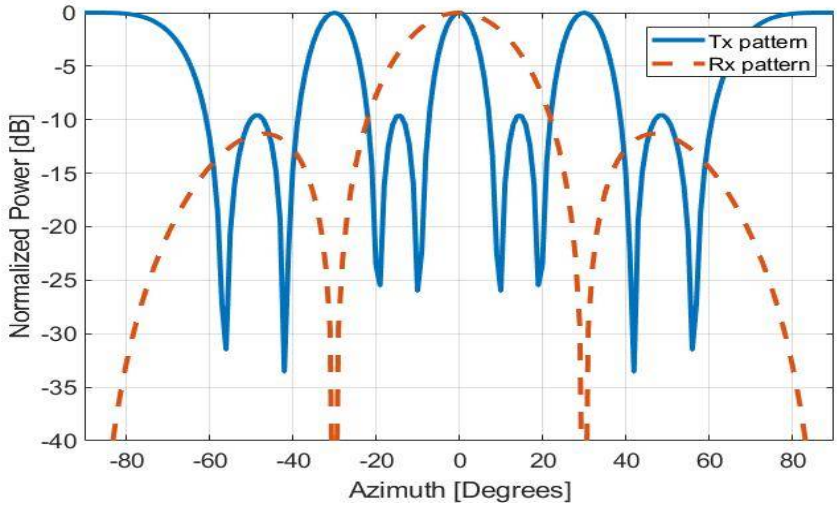

Figure 2.2: Tx and Rx patterns for the 3 Tx and 4 Rx antenna system

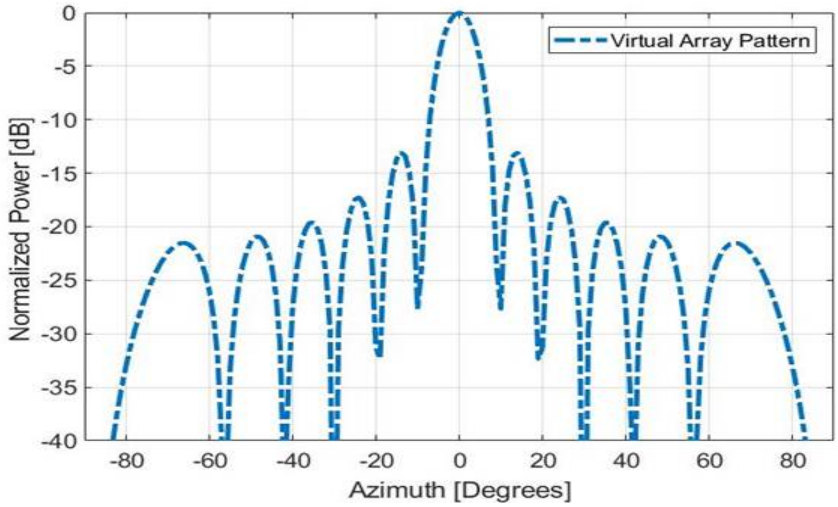

Figure 2.3: Virtual array pattern for the 3 Tx and 4 Rx antenna system

If the above design is looked at from the perspective of improving angular resolution and rejection capabilities, while keeping the thermal noise in mind, the 4 Rx channels can be increased to 8 Rx channels. Doing so will double the number of interference signals that can be suppressed by beamforming, will double the number of virtual array elements and the main lobe width will be reduced by half, thus making the automotive radar more accurate.

2.2. MIMO BEAMFORMING

Beamforming or spatial filtering is a signal processing technique used in radar for directional transmission or reception of the signal. Beamforming can be achieved by changing the amplitude and the phase shifts of the antenna array elements also known as weights in such a way that the main beam of the antenna array is directed towards the desired direction and maximum amount of power is transmitted or received in that particular direction.

For a MIMO radar, the beamforming techniques will be applied on the virtual array data vector. So the weights calculation for the beamformers will be done using the virtual array steering vector given in equation 2.10. As mentioned before beamforming is done to maximize the SNR in a particular direction, in our discussion we will look into conventional and adaptive beamformers. The signal model in equation 2.10 will be used to derive the beamformers.

2.2.1. CONVENTIONAL BEAMFORMERS

The conventional beamformers have only one goal function and that is to maximize the SNR of the signal coming from a particular direction. If the signal is surrounded by nothing else than white Gaussian noise, than the conventional beamformer will be considered an optimal beamformer as it will be able to provide the highest achievable output SNR. For this reason the conventional beamformer is the mostly used beamformer in antenna array systems. In MIMO systems when using the conventional beamformer, the weights will be similar to the steering vector of the virtual array.

$$\boldsymbol{w}_{conv} = \boldsymbol{v}(\theta_t) \tag{2.14}$$

The reason for this is that the beamformer will only look to maximize the SNR at the output, so it will only steer the main beam towards the target and try to receive as much power from the target signal it can. But when the target is in the background of interference signals and the powers of these interference signals are much higher than the power of the target signal, the conventional beamformer will not perform optimally, resulting in target signal being lost.

2.2.2. ADAPTIVE BEAMFORMERS

The purpose of an adaptive beamformer is to maximize the signal response and simultaneously minimize the interference and noise response. We can use equation 2.10 for our task of beamforming with interference suppression. From equation 2.10

$$\boldsymbol{y} = \alpha_t \boldsymbol{v}(\theta_t) + \boldsymbol{y}_i + \boldsymbol{n} \tag{2.15}$$

The term $\alpha_t \boldsymbol{v}(\theta_t)$ is the desired signal and $E\{|\ \alpha_t\ |^2\} = \sigma_t^2$, the term $\boldsymbol{y}_i$ represents the interference signals form J different interference sources and $\boldsymbol{n}$ is the white Gaussian noise, where $E\{|\ nn^H\ |^2\} = \sigma_n^2$. From equation 2.16, the interference and noise signals can be given by:

$$\boldsymbol{y}_{i+n} = \boldsymbol{y}_i + \boldsymbol{n} \tag{2.16}$$

And the covariance matrix for the interference signal and noise is defined as:

$$\boldsymbol{R}_{i+n} = E\{|\ \boldsymbol{y}_{i+n}\boldsymbol{y}_{i+n}^H\ |^2\} = \boldsymbol{R}_{y_i} + \boldsymbol{R}_n \tag{2.17}$$

Where $\boldsymbol{R}_{y_i} = E\{|\ \boldsymbol{y}_i \boldsymbol{y}_i^H\ |^2\}$ is the covariance matrix of the interference signal and $\boldsymbol{R}_i = E\{|\ \boldsymbol{n}\boldsymbol{n}^H\ |^2\}$ is the covariance matrix of the noise. Using equation 2.18, the covariance for the incoming signal in equation 2.16 can be defined as:

$$\boldsymbol{R} = E\{\boldsymbol{y}\boldsymbol{y}^H\} = \sigma_t^2 \boldsymbol{v}(\theta_t)\boldsymbol{v}^H(\theta_t) + \boldsymbol{R}_{y_i} + \boldsymbol{R}_n \tag{2.18}$$

If the signal power is σ_t^2, the power of the *ith* interference source is σ_i^2 and noise power is given by σ_n^2, the SINR at the output of the radar can be given by:

$$SINR = \frac{\sigma_t^2}{\sum_{i=1}^{J} \sigma_i^2 + \sigma_n^2} \tag{2.19}$$

For an adaptive weight vector $\boldsymbol{w}$, the SINR at the beamformer output is:

$$SINR = \frac{E\{\boldsymbol{w}^H \boldsymbol{y}_t \boldsymbol{y}_t^H \boldsymbol{w}\}}{E\{\boldsymbol{w}^H \boldsymbol{y}_{i+n} \boldsymbol{y}_{i+n}^H \boldsymbol{w}\}} \tag{2.20}$$

$$SINR = \frac{\boldsymbol{w}^H \boldsymbol{R}_t \boldsymbol{w}}{\boldsymbol{w}^H \boldsymbol{R}_{i+n} \boldsymbol{w}} \tag{2.21}$$

where $\boldsymbol{R}_t = E\{\boldsymbol{y}_t \boldsymbol{y}_t^H\}$ is the covariance matrix of the target signal $\boldsymbol{y}_t = \alpha_t \boldsymbol{v}(\theta_t)$.

The adaptive beamformer will generate a weight vector $\boldsymbol{w}$ to minimize the interference plus noise at the output of the beamformer while keeping the term $\boldsymbol{w}^H \boldsymbol{R}_t \boldsymbol{w}$ constant, maximizing the SINR at the beamformer output given by equation 2.22. This type of adaptive beamformer is known as the MVDR (Minimum Variance Distortionless Response) beamformer. The MVDR beamformer can be expressed in the form of following optimization problem:

$$\begin{array}{ll} \min_{\boldsymbol{w}} & \boldsymbol{w}^H \boldsymbol{R}_{i+n} \boldsymbol{w} \\ s.t & \boldsymbol{w}^H \boldsymbol{v}(\theta_t) = 1 \end{array} \tag{2.22}$$

The above constrained optimization problem can be transformed into an unconstrained one by using the method of Lagrange multipliers. The Lagrangian function for the optimization problem can be written as:

$$\mathscr{L}(\boldsymbol{w}, \lambda) = \boldsymbol{w}^H \boldsymbol{R}_{i+n} \boldsymbol{w} + \lambda(1 - \boldsymbol{w}^H \boldsymbol{v}(\theta_t)) \tag{2.23}$$

Computing the gradient for the Lagrangian given by equation 2.23 and equating to zero yield,

$$\nabla \mathscr{L}(\boldsymbol{w}, \lambda)_{\boldsymbol{w}} = \boldsymbol{R}_{i+n} \boldsymbol{w} - \lambda \boldsymbol{v}(\theta_t) = 0 \tag{2.24}$$

Rearranging for $\boldsymbol{w}$,

$$\boldsymbol{w} = \lambda \boldsymbol{R}_{i+n}^{-1} \boldsymbol{v}(\theta_t) \tag{2.25}$$

Substituting 2.25 into the constraint of equation 2.22 and solving for λ,

$$\lambda = \frac{1}{\boldsymbol{v}^H(\theta_t) \boldsymbol{R}_{i+n}^{-1} \boldsymbol{v}(\theta_t)} \tag{2.26}$$

Substituting equation 2.26 in 2.25 , and solving for $\boldsymbol{w}$ we have,

$$\boldsymbol{w} = \frac{\boldsymbol{R}_{i+n}^{-1}\boldsymbol{v}(\theta_t)}{\boldsymbol{v}^H(\theta_t)\boldsymbol{R}_{i+n}^{-1}\boldsymbol{v}(\theta_t)} \tag{2.27}$$

The weight vector calculated using equation 2.27 can be used to recover the target signal $\boldsymbol{y}_t$, by multiplying the weight vector by the received signal in equation 2.16. The improvement after applying the calculated adapted weight vector from equation 2.27 can be described by the SINR. If the power of the target signal is σ_t^2 and the direction dependant virtual array steering vector is $\boldsymbol{v}(\theta_t)$, and interference and noise adds to the signal, the SINR at the beamformer output is:

$$SINR = \frac{\sigma_t^2 \mid \boldsymbol{w}^H\boldsymbol{v}(\theta_t) \mid^2}{\boldsymbol{w}^H\boldsymbol{R}_{i+n}\boldsymbol{w}} \tag{2.28}$$

The interference plus noise covariance matrix is given by:

$$\boldsymbol{R}_{i+n} = \sum_{i=1}^{J} \sigma_i^2 \boldsymbol{v}(\theta_i)\boldsymbol{v}^H(\theta_i) + \sigma_n^2\boldsymbol{I} \tag{2.29}$$

where σ_i^2 is the variance of the signal from the *ith* interference source. Substituting equation 2.29 in 2.28 we have

$$SINR = \frac{\sigma_t^2 \mid \boldsymbol{w}^H\boldsymbol{v}(\theta_t) \mid^2}{\boldsymbol{w}(\sum_{i=1}^{J} \sigma_i^2 \boldsymbol{v}(\theta_i)\boldsymbol{v}^H(\theta_i) + \sigma_n^2\boldsymbol{I})\boldsymbol{w}} \tag{2.30}$$

The SINR expression in the equation 2.30 will used as a metric of performance measure for various antenna designs. We can see from the equation that the SINR is dependent on the steering vectors of the virtual array, and from the expression of the steering vector in equation 2.12 we can say that the positions of the antenna elements will play a important role in improving or degrading the SINR at the output.

SAMPLE MATRIX ESTIMATION

In practice the matrix $\boldsymbol{R}_{i+n}$ is unknown and therefore must be estimated. The covariance matrix can be estimated from Z data snapshots $\boldsymbol{y}_z$ at the virtual array output by:

$$\hat{\boldsymbol{R}} = \frac{1}{Z}\sum_{z=1}^{Z} \boldsymbol{y}_z\boldsymbol{y}_z^H \tag{2.31}$$

The estimated $\hat{\boldsymbol{R}}$ is inverted and applied in equation 2.27 to calculate the values of the beamformer weights $\boldsymbol{w}$. This method of matrix estimation and calculating weights is known as sample matrix inversion method (SMI) and the estimated covariance matrix is known as sample covariance matrix.

Replacing $\boldsymbol{R}_{i+n}^{-1}$ by $\hat{\boldsymbol{R}}^{-1}$, the expression for weight computation can rewritten as:

$$\boldsymbol{w} = \frac{\hat{\boldsymbol{R}}^{-1}\boldsymbol{v}(\theta_t)}{\boldsymbol{v}^H(\theta_t)\hat{\boldsymbol{R}}^{-1}\boldsymbol{v}(\theta_t)} \tag{2.32}$$

Note that the target signal component is present in $\hat{\boldsymbol{R}}$. An alternative way to obtain a target signal free sample covariance matrix is to collect the data snapshots $\boldsymbol{y}_z$ for Z different range bins. For our work we will use the second approach to estimate the covariance matrix.

The advantage of the adaptive beamformer over the conventional beamformer in the presence of power full interference signals can be illustrated by using equation 2.30 to compute the output SINR. To illustrate this advantage of the adaptive beamformer over the conventional beamformer, we assume for a MIMO system 3 Tx channels and 4 Rx channels, two interference sources at -30° and -10° and the target at 10°. The noise power is assumed to be 1W and the interference signal at the Rx array power is assumed to be 30dB and the target signal power at the Rx array power is varied from -50dB to 50dB. The sample Covariance matrix is computed based on Z=100 data snapshots, which will result in a matrix of size 12×12. Figures 2.4 and 2.5 show the MIMO beam patterns after the beamformer weights are applied, and figure 2.6 shows the output SINR's for adaptive (MVDR) and the conventional beamformer.

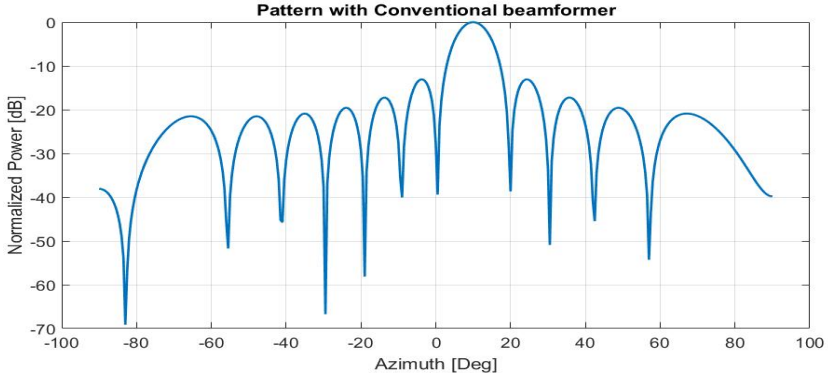

Figure 2.4: MIMO Pattern for Conventional beamformer, target at 10° and interference sources at -30° and -10°

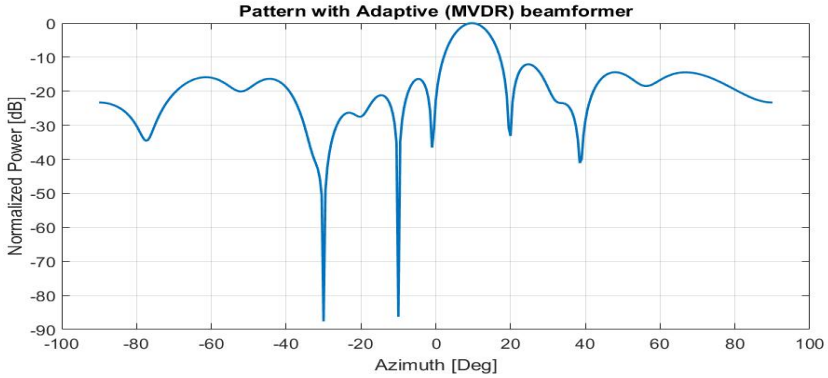

Figure 2.5: MIMO Pattern for Adaptive beamformer, target at 10° and interference sources at -30° and -10°

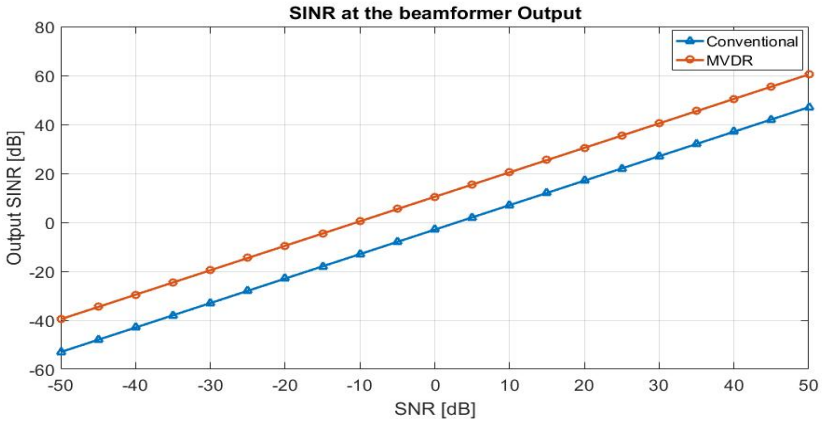

Figure 2.6: Output SINR of the Conventional and Adaptive(MVDR) beamformer for target at 10° and interference sources at -30° and -10°

From figures 2.4 and 2.5, we see that the conventional beamformer is focused on maximizing the SNR in the direction of the target and pays no attention to the interference signals incident on the Rx array, while the adaptive (MVDR) beamformer focuses on minimizing the interference response and simultaneously maximizing the target response, that is why in figure 2.5, we see pattern notches/nulls in the direction of the interference signals. Figure 2.6 confirms the superiority of the adaptive beamformer, as we can see an improvement of 13.41dB in the output SINR for the adaptive beamformer compared to the conventional beamformer.

2.3. CONCLUSION

In this chapter, a MIMO signal model in the presence of multiple interference sources is formulated. The MIMO virtual array in the signal model is created by using orthogonal waveforms that are simultaneously transmitted from the Tx array and the echos of these orthogonal waveforms are received and can be affiliated to the transmit element that radiated that waveform.

An adaptive beamformer is derived, as the conventional beamformer (steering the main beam towards the target) is optimal only when the target is in the presence of white Gaussian noise. For the weights of the adaptive beamformer the covariance matrix for interference plus noise is estimated via the method of Sample Matrix Inversion (SMI). Using the derived adaptive beamformer in a scenario of a target at 10° and two interference sources at -30° and -10° results in an improvement of 13.41dB over the conventional beamformer.

The MIMO signal model along with the adaptive beamformer from this chapter will be used in chapter 4 to test the performance of the antenna array topologies that will be designed in chapter 3, in the presence of multiple interference sources. The output SINR of the adaptive beamformer from equation 2.30, will be used as a metric for ranking the performance for various antenna topologies.

3

ANTENNA ARRAY TOPOLOGY

This chapter describes two techniques to design a suitable antenna topology for improving the performance of the MIMO system at the output of the adaptive beamformer. The first section describes a thinning strategy where some antenna elements are turned off to obtain the array topology that generates a suitable pattern. The second section describes the Multi beam optimization technique, where a non-uniform MIMO array is synthesized for low sidelobes while scanning at various angles and the third section describes how the pattern of the non-uniform MIMO array is factorized to obtain the transmit and receive pattern which in turn will be used to determine the positions of the transmit and receive antenna positions.

3.1. THINNING STRATEGY

The thinning strategy used in this work will be used to design the virtual array of the MIMO system. The pattern of the designed virtual array will then be factorized to obtain the pattern of the Tx and Rx arrays for the MIMO system. The thinning strategy will use the radiation patterns for several possible topologies to check which ones satisfy the set constraints. The final result may result in more than one topology. The best topologies using the thinning of the array are determined via the following five steps:

STEP 1

1. Select the aperture size of K elements on which the receiver array of N no of elements will be placed, while $K > N$.

2. Create an uniformly spaced array with spacing $\lambda/2$ of K elements, and create on and off sequences for the array of K elements. Which will result in $M = 2^K - 1$ possible sequences.

3. Out of these M sequences select the sequences with the aperture efficiency:

$$\eta = \frac{N}{K} \tag{3.1}$$

Place the sequences with the aperture efficiency η, in the set J.

4. Choose a value of the sidelobe threshold SLL_{th}

STEP 2

The set J will have $H = \binom{N}{K}$ no of sequences, For these H sequences the array factor of the hth sequence can be expressed as:

$$AF^{(h)}(\theta) = \frac{\sum_{k=1}^{K} I_k^{(h)} e^{-j\beta(k-1)d\cos\theta}}{\sum_{k=1}^{K} I_k^{(h)}} \tag{3.2}$$

where $\beta = 2\pi/\lambda$ is the free-space wavenumber, and θ is angle from the array axis. $I_k^{(h)}$ is the status of the kth element for the hth sequence. If the kth element is on for the hth sequence $I_k^{(h)} = 1$ and if off, $I_k^{(h)} = 0$. d is the inter element distance of the uniform array of K elements, in this case $d = \lambda/2$.

Out of these H sequences keep only those sequences whose peak sidelobes levels PSL are smaller than the PSL of the uniformly spaced array of N elements.

$$PSL^{(h)} < PSL_{ULA} = \frac{1}{N \sin\frac{3\pi}{2N}} \tag{3.3}$$

Place the sequences that satisfy equation 3.3 in set A.

STEP 3

For each sequence from the set A, generate a vector $\theta_{null}^{(a)}$ of angular positions where the value of the array factor is below the set sidelobe threshold SLL_{th} excluding the main lobe.

$$\theta_i \in \theta_{null}^{(a)} \leftrightarrow |\lfloor AF^{(h)}(\theta_i)\rfloor_{\theta_i \notin R_M}|^2 < SLL_{th} \tag{3.4}$$

We call this vector of angular positions a nulling vector. θ_i, where $i = 1,,,,,,I$ being the ith sample of the whole angular region ($\theta_i = -\pi/2$ and $\theta_I = \pi/2$). R_M is the main lobe region.

STEP 4

From the set of A sequences select those for which the SLL for all the angles is below SLL_{th} ,in other words, select the sequences for which the Nulling region contains all the angles expect the main lobe region:

$$\lfloor \theta_i = \theta_{full} \rfloor_{\theta_i \notin R_M, \theta_{full} \notin R_M} \tag{3.5}$$

Where θ_{full} is the vector of all the angular positions excluding the main lobe. Place the sequences from A satisfying equation 3.5 in the set Q.

STEP 5

Within Q there may be some sequences which generate the same pattern. Remove the sequences with repeating patterns, place the remaining sequences in the control set R. The Sequences or topologies in the control set are the final topologies for the receiver array of MIMO system.

The sequences or topologies from the control set R along with the MIMO model and the adaptive beamformer will be implemented in MATLAB to check the performance of the topology and compare it with the performance of ULA.

3.2. MULTI BEAM OPTIMIZATION TECHNIQUE

The multi beam optimization technique, designs an array by moving the elements of a uniformly spaced array in such a way that the array will have low sidelobes even when the main beam is scanned at various angles. The new positions of the array elements are determined by using an iterative convex optimization problem, that keeps on repeating until the sidelobes cannot be reduced any further. This section described the formulation of the iterative optimization problem.

3.2.1. FORMULATION OF THE OPTIMIZATION PROBLEM

For formulating the problem , consider an array of N elements with uniform inter element distance. The radiation pattern of the array can be given by:

$$RP(\theta) = \sum_{n=1}^{N} P_n(\theta) e^{j\beta\cos\theta x_n} \tag{3.6}$$

where $\beta = 2\pi/\lambda$, x_n is the position of the nth element of the array, θ is the angle from the array Axis and $P_n(\theta)$ is the filed radiated by the nth element of the array. If the radiated filed for each element of the array is same, the radiation pattern of the array becomes:

$$RP(\theta) = P(\theta) \sum_{n=1}^{N} e^{j\beta\cos\theta x_n} \tag{3.7}$$

Using the iterative method of [28], we start with a uniform linear array with spacing d_{ini} and move the nth element by ϵ_n^i at the ith iteration of the convex problem, the new position of the nth element is

$$x_n^i = x_n^{i-1} + \epsilon_n^i \tag{3.8}$$

Substituting 3.8 into 3.7 the expression of the radiation pattern becomes,

$$RP(\theta) = P(\theta) \sum_{n=1}^{N} e^{j\beta\cos\theta(x_n^{i-1}+\epsilon_n^i)} \tag{3.9}$$

$$RP(\theta) = P(\theta) \sum_{n=1}^{N} e^{j\beta\cos\theta x_n^{i-1} + j\beta\cos\theta\epsilon_n^i} \tag{3.10}$$

$$RP(\theta) = P(\theta) \sum_{n=1}^{N} e^{j\beta\cos\theta x_n^{i-1}} e^{j\beta\cos\theta\epsilon_n^i} \tag{3.11}$$

The expression in equation 3.11 does not linearly depend on the increment in the position of the elements (ϵ_n^i), which will result in an optimization problem that is not convex. This problem is overcame by using the Taylor expansion $e^{j\phi} = 1 + j\phi$, where $\phi = \beta\cos\theta\epsilon_n^i$, and the expression of the radiation pattern in equation 3.11 is linearized around the element locations. Thus the radiation pattern for the ith iteration can be written as:

$$RP_{\epsilon_n}^i(\theta) \approx P(\theta)\sum_{n=1}^{N} e^{j\beta\cos\theta(x_n^{i-1})}(1 + j\beta\cos\theta\epsilon_n^i) \tag{3.12}$$

In general, equation 3.12 is a good approximation of the pattern in equation 3.11, provided that the increment (ϵ_n^i) is much smaller than $\lambda/(2\pi)$:

$$|\beta\cos\theta\epsilon_n^i| \ll 1 \quad i.e. |\epsilon_n^i| \ll \lambda/2\pi = 0.16\lambda \tag{3.13}$$

Assuming a scenario where the main beam of the array is scanned at l different angles. θ_s represents the scan angle, where $s = 1, 2, \ldots, l$. The phase shift at the nth element for the scan angle θ_s for the ith iteration can be expressed as:

$$\psi_{n,s}^i = e^{-j\beta\cos\theta_s x_n^i} \tag{3.14}$$

The radiation pattern in equation 3.7 for scanning the main beam at ith iteration can be written as:

$$RP^{i,s}(\theta) = P(\theta)\sum_{n=1}^{N} e^{j\beta\cos\theta x_n^i}\psi_{n,s}^i \tag{3.15}$$

Substituting 3.14 into 3.15, the expression for the radiation pattern becomes,

$$RP(\theta) = P(\theta)\sum_{n=1}^{N} e^{j\beta\cos\theta x_n^i}e^{-j\beta\cos\theta_s x_n^i} \tag{3.16}$$

$$RP(\theta) = P(\theta)\sum_{n=1}^{N} e^{j\beta(\cos\theta-\cos\theta_s)x_n^i} \tag{3.17}$$

Substituting 3.8 into 3.17 and using the Taylor expansion $e^{j\phi} = 1 + j\phi$, where $\phi = \beta\cos\theta\epsilon_n^i$, the expression for the radiation pattern for a scanned beam at the ith iteration can be expressed as:

$$RP_{\epsilon_n}^{i,s}(\theta) \approx P(\theta)\sum_{n=1}^{N} e^{j\beta(\cos\theta-\cos\theta_s)x_n^{i-1}}(1 + j\beta\cos\theta\epsilon_n^i)(1 - j\beta\cos\theta_s\epsilon_n^i) \tag{3.18}$$

Ignoring the higher-order terms in 3.18, we obtain the following expression, which can be used at each iteration of the convex optimization algorithm.

$$RP_{\epsilon_n}^{i,s}(\theta) \approx P(\theta)\sum_{n=1}^{N} e^{j\beta(\cos\theta-\cos\theta_s)x_n^{i-1}}(1 + j\beta(\cos\theta - \cos\theta_s)\epsilon_n^i) \tag{3.19}$$

The positions of the array elements for the ith iteration are given by:

$$x^i = [x_1^i, x_2^i, \ldots\ldots\ldots\ldots, x_N^i]^T \tag{3.20}$$

The change in positions for the array elements for the ith iteration are given by the following vector:

$$\epsilon^i = [\epsilon_1^i, \epsilon_2^i, ..., \epsilon_N^i]^T \tag{3.21}$$

the l scan angles are given by the following vector:

$$\theta_s = [\theta_1, \theta_2, ..., \theta_l] \tag{3.22}$$

The sidelobe region for the scan angle is determined according to pre-specified beam width, θ_b such that,

$$\theta \in \theta_{SL,s} if \theta < (\theta_s - \theta_b) or (\theta) > (\theta_s - \theta_b) \tag{3.23}$$

Using 3.23, the sidelobe regions for each scan angle can be given by the following vector:

$$\theta_{SL,s} = [\theta_{SL,1}, \theta_{SL,2}, ..., \theta_{SL,l}] \tag{3.24}$$

To calculate the inter-element distance at each iteration a $(N-1) \times N$ circulant matrix D is formed.

$$\begin{bmatrix} -1 & 1 & 0 & 0 & \dots & 0 & 0 & 0 \\ 0 & -1 & 1 & 0 & \dots & 0 & 0 & 0 \\ 0 & \ddots & \ddots & \ddots & \ddots & \ddots & \ddots & \vdots \\ \vdots & \ddots & \ddots & \ddots & \ddots & -1 & 1 & 0 \\ 0 & 0 & 0 & 0 & 0 & 0 & -1 & 1 \end{bmatrix} \tag{3.25}$$

Using the radiation pattern form equation 3.19 and the vectors from 3.20, 3.21, 3.22,3.23,3.24 and 3.25, we can formulate a iteration based convex optimization problem. At each iteration the following convex optimization problem will be solved:

$$\begin{aligned} \min_{\epsilon^i} \quad & SLL \\ \text{s.t.} \quad & \max | RP_{\epsilon^i}^{\theta_s, i}(\theta_{SL,s}) | \leq SLL \\ & | \epsilon^i | \leq \mu \\ & D * (\epsilon^i + x^{i-1}) \geq d_{min} \end{aligned} \tag{3.26}$$

Where SLL is the maximum sidelobe level which is minimized for all the defined scan angles. $| \epsilon^i |$ is upper-bounded by 0.16λ, this upper bound is decided based on equation 3.13. The last constraint guarantees that the inter element distance at each iteration is less than or equal to the desired value d_{min}.

The optimization problem in equation 3.26 is a second order cone program and can be solved using interior-point method by many readily available solvers. In this thesis the optimization problem is solved using the CVX solver and will be used to synthesize a non-uniform MIMO virtual array. The array will be optimized to obtain low sidelobes for a predefined scan range.

From the optimization problem the positions of the virtual array elements that generate the optimal pattern with low sidelobes are obtained and that pattern can be factorized to achieve the patterns of the Transmitter and Receiver array, from which the positions of the elements for the Tx and Rx array elements can be extracted.

3.3. POLYNOMIAL FACTORIZATION

This section is divided in two parts, the first part explains the general factorization method and the second part explains how the general factorization method can be used to factorize the virtual array radiation pattern to obtain the Tx and Rx arrangements using two design examples.

3.3.1. GENERAL POLYNOMIAL FACTORIZATION METHOD

Consider a polynomial $P_L(x)$ of degree L in positive powers of x and with unity coefficients [29],[30],[31].

$$P_L(x) = \sum_{j=1}^{L} x^j \tag{3.27}$$

The number of coefficients in $P_L(x)$ can be given by a positive integer $L+1$. Let the positive number $L+1$ be expressed as a product of $G+1$ irreducible positive integers $L_g+1, 0 \leq g \leq G$

$$L+1 = \prod_{g=0}^{G} (L_G+1) \tag{3.28}$$

Then $P_L(x)$ can be expressed in the from [29],[31]

$$P_L(x) = \prod_{g=0}^{G} P_{L_g}(x^{S_g}) \tag{3.29}$$

Where

$$S_g = \prod_{h=0}^{g} (L_{h-1}+1) \tag{3.30}$$

Where $L_{-1} = 0$.

The factorization of the specified number $L+1$ into a product of $G+1$ irreducible integers can be carried out by using Euclid's algorithm. In the case when $L+1$ can be expressed as a power of two, that is,

$$L+1 = 2^{\gamma} \tag{3.31}$$

Where γ is an integer, then $P_L(x)$ will be factorized as,

$$P_L(x) = (1+x)(1+x^2).....(1+x^{2\gamma-1}) \tag{3.32}$$

3.3.2. PATTERN FACTORIZATION AND DESIGN EXAMPLES

Consider a MIMO system with M Tx elements and N Rx elements, the Tx and Rx pattern can be given as:

$$P_T(\theta) = \sum_{m=1}^{M} e^{j2\pi \frac{x_m}{\lambda} \sin\theta} \tag{3.33}$$

$$P_R(\theta) = \sum_{n=1}^{N} e^{j2\pi \frac{x_n}{\lambda} \sin\theta} \tag{3.34}$$

Where x_m and x_n are the positions of Tx and Rx elements. The pattern of a MIMO virtual array can be written as the product of the Tx and Rx patterns.

$$P_V(\theta) = P_T(\theta)P_R(\theta) \tag{3.35}$$

$$P_V(\theta) = \sum_{m=1}^{M} e^{j2\pi \frac{x_m}{\lambda} \sin\theta} \sum_{n=1}^{N} e^{j2\pi \frac{x_n}{\lambda} \sin\theta} \tag{3.36}$$

$$P_V(\theta) = \sum_{m=1}^{M} \sum_{n=1}^{N} e^{j2\pi \frac{x_m + x_n}{\lambda} \sin\theta} \tag{3.37}$$

Substituting $x = e^{j2\pi \frac{d}{\lambda} \sin\theta}$, with d being the inter-element distance, The Tx, Rx and the virtual array pattern can be written as:

$$P_V(x) = \sum_{i=0}^{MN-1} x^i \tag{3.38}$$

$$P_V(x) = \sum_{i=0}^{M} x^i \tag{3.39}$$

$$P_V(x) = \sum_{i=0}^{N} x^i \tag{3.40}$$

$$P_V(x) = P_T(x)P_R(x) \tag{3.41}$$

We can design the transmit and receive arrays based on factorizing the desired MIMO virtual array polynomial $P_V(x)$ as product of two lower order polynomials, using the polynomial factorization method.

Using the above mentioned factorization method of the virtual array pattern, two designs are considered, MIMO virtual array of 12 elements and MIMO virtual array of 24 elements. The pattern of the resulting arrays will then be factorized to obtain the patterns for Tx and Rx arrays, which in turn will be used to find the locations of the array elements in an x-y coordinate system.

MIMO VIRTUAL ARRAY OF 12 ELEMENTS

The radiation pattern of the virtual array is given by:

$$P_V(x) = \sum_{i=0}^{MN-1} x^i \tag{3.42}$$

$$P_V(x) = 1 + x + x^2 + x^3 + x^4 + x^5 + x^6 + x^7 + x^8 + x^9 + x^{10} + x^{11} \tag{3.43}$$

Where $x = e^{j2\pi \frac{d}{\lambda} \sin\theta}$. For this design $MN = 12$, using the Euclid's algorithm we can express 12 into the product of three irreducible integers i.e.$12 = 2 \times 2 \times 3$,and by changing the arrangements of theses irreducible integers and using equations 3.29 and 3.30, the virtual array pattern in equation 3.43 can be factorized in the following three ways:

FACTORIZATION 1:
For the arrangement, $12 = 2 \times 2 \times 3$, using equation 3.29 and 3.30 the virtual array pattern can be factorized as:

$$P_V(x) = (1+x)(1+x^2)(1+x^4+x^8) \tag{3.44}$$

FACTORIZATION 2:
For the arrangement, $12 = 2 \times 3 \times 2$, using equation 3.29 and 3.30 the virtual array pattern can be factorized as:

$$P_V(x) = (1+x)(1+x^2+x^4)(1+x^6) \tag{3.45}$$

FACTORIZATION 3:
For the arrangement, $12 = 3 \times 2 \times 2$, using equation 3.29 and 3.30 the virtual array pattern can be factorized as:

$$P_V(x) = (1+x+x^2)(1+x^3)(1+x^6) \tag{3.46}$$

From the three factorizations of the virtual array pattern (Equation 3.44-Equation 3.46), there are nine possible Tx-Rx patterns. Table 3.1 shows the nine possible Tx and Rx designs corresponding to the three factorizations of the virtual array pattern.

Design	$P_T(x)$	$P_R(x)$	N_T	N_R
1	$1+x$	$1+x^2+x^4+x^6+x^8+x^{10}$	2	6
2	$1+x^2$	$1+x+x^4+x^5+x^8+x^9$	2	6
3	$1+x^4+x^8$	$1+x+x^2+x^3$	3	4
4	$1+x$	$1+x^2+x^4+x^6+x^8+x^{10}$	2	6
5	$1+x^2+x^4$	$1+x+x^6+x^7$	3	4
6	$1+x^6$	$1+x^2+x^3+x^4+x^5+x^6$	2	6
7	$1+x+x^2$	$1+x^3+x^6+x^9$	3	4
8	$1+x^3$	$1+x+x^2+x^6+x^7+x^8$	2	6
9	$1+x^6$	$1+x+x^2+x^3+x^4+x^5$	2	6

Table 3.1: Transmit and Receive Patterns for the nine designs obtained by factorizing the Virtual array Pattern

Figures 3.1, 3.2 and 3.3 shows the antenna arrangements for the nine Tx-Rx arrays designs shown in table 3.1.

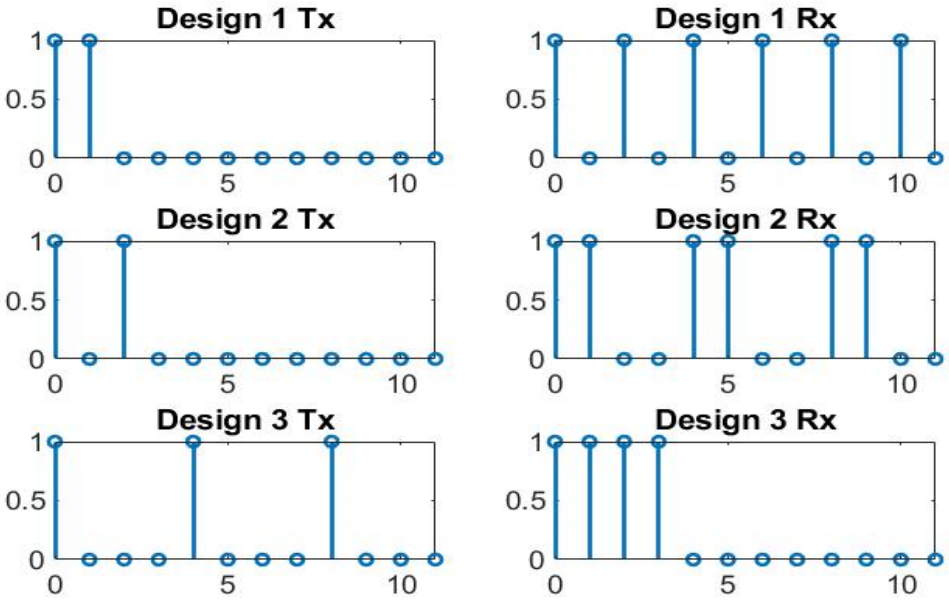

Figure 3.1: Antenna Arrangements for the Tx and Rx designs from factorization 1, 1 indicates there is an antenna and 0 indicates the absence of the antenna

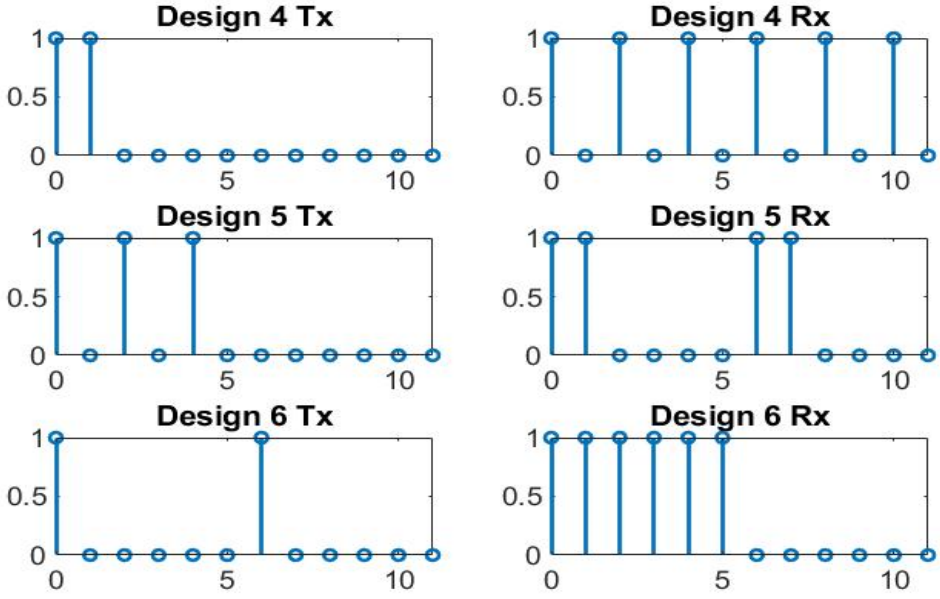

Figure 3.2: Antenna Arrangements for the Tx and Rx designs from factorization 2, 1 indicates there is an antenna and 0 indicates the absence of the antenna

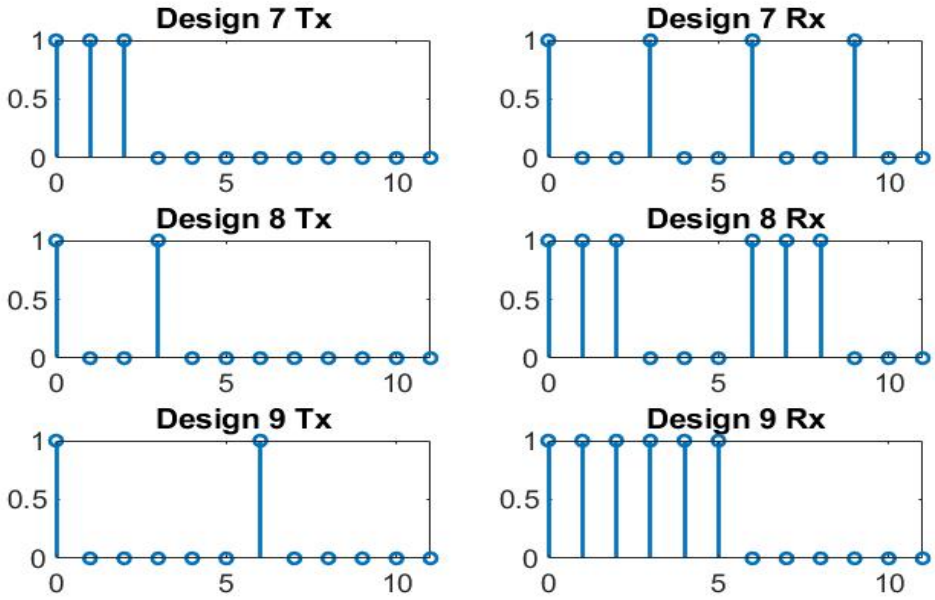

Figure 3.3: Antenna Arrangements for the Tx and Rx designs from factorization 3, 1 indicates there is an antenna and 0 indicates the absence of the antenna

MIMO VIRTUAL ARRAY OF 24 ELEMENTS

Using the same steps as Design for 12 elements we can factorize the pattern of the virtual array and obtain the Tx-Rx array designs. The pattern of the virtual array can be given by:

$$P_V(x) = \sum_{i=0}^{MN-1} x^i \tag{3.47}$$

$$\begin{aligned} P_V(x) = 1 + x + x^2 + x^3 + x^4 + x^5 + x^6 + x^7 + x^8 + x^9 + x^{10} + x^{11} + x^{12} \\ + x^{13} + x^{14} + x^{15} + x^{16} + x^{17} + x^{18} + x^{19} + x^{20} + x^{21} + x^{22} + x^{23} \end{aligned} \tag{3.48}$$

For this case $MN = 24$, using the Euclid's algorithm we can express 12 into the product of four irreducible integers i.e.$24 = 2 \times 2 \times 3 \times 2$,and by changing the arrangements of theses irreducible integers and using equations 3.29 and 3.30, the virtual array pattern in equation 3.48 can be factorized in the following four ways:

FACTORIZATION 1:

For the arrangement, $24 = 2 \times 3 \times 2 \times 2$, using equation 3.29 and 3.30 the virtual array pattern can be factorized as:

$$P_V(x) = (1 + x)(1 + x^2 + x^4)(1 + x^6)(1 + x^{12}) \tag{3.49}$$

FACTORIZATION 2:
For the arrangement, $24 = 3 \times 2 \times 2 \times 2$, using equation 3.29 and 3.30 the virtual array pattern can be factorized as:

$$P_V(x) = (1 + x + x^2)(1 + x^3)(1 + x^6)(1 + x^{12}) \tag{3.50}$$

FACTORIZATION 3:
For the arrangement, $24 = 2 \times 2 \times 3 \times 2$, using equation 3.29 and 3.30 the virtual array pattern can be factorized as:

$$P_V(x) = (1 + x)(1 + x^2)(1 + +x^4 + x^6)(1 + x^{12}) \tag{3.51}$$

FACTORIZATION 4:
For the arrangement, $24 = 2 \times 2 \times 2 \times 3$, using equation 3.29 and 3.30 the virtual array pattern can be factorized as:

$$P_V(x) = (1 + x)(1 + x^2)(1 + x^4)(1 + x^8 + x^{12}) \tag{3.52}$$

From the above four factorizations of the virtual array pattern (Equations 3.49-3.52), there are 16 possible Tx-Rx designs. Table 3.2 shows the 16 possible Tx and Rx designs corresponding to the factorizations of the virtual array pattern.

Design	$P_T(x)$	$P_R(x)$	N_T	N_R
1	$(1 + x + x^2)$	$(1 + x^3)(1 + x^6)(1 + x^{12})$	3	8
2	$(1 + x^3)$	$(1 + x + x^2)(1 + x^6)(1 + x^{12})$	2	12
3	$(1 + x^6)$	$(1 + x + x^2)(1 + x^3)(1 + x^{12})$	2	12
4	$(1 + x^{12})$	$(1 + x + x^2)(1 + x^3)(1 + x^6)$	2	12
5	$(1 + x + x^2)$	$(1 + x^3)(1 + x^6)(1 + x^{12})$	3	8
6	$(1 + x^3)$	$(1 + x + x^2)(1 + x^6)(1 + x^{12})$	2	12
7	$(1 + x^6)$	$(1 + x + x^2)(1 + x^3)(1 + x^{12})$	2	12
8	$(1 + x^{12})$	$(1 + x + x^2)(1 + x^3)(1 + x^6)$	2	12
9	$(1 + x^4 + x^8)$	$(1 + x)(1 + x^2)(1 + x^{12})$	3	8
10	$(1 + x)$	$(1 + x^2)(1 + x^4 + x^8)(1 + x^{12})$	2	12
11	$(1 + x^2)$	$(1 + x)(1 + x^4 + x^8)(1 + x^{12})$	2	12
12	$(1 + x^{12})$	$(1 + x)(1 + x^2)(1 + x^4 + x^8)$	2	12
13	$(1 + x^8 + x^{16})$	$(1 + x)(1 + x^2)(1 + x^4)$	3	8
14	$(1 + x)$	$(1 + x^2)(1 + x^4)(1 + x^8 + x^{16})$	2	12
15	$(1 + x^2)$	$(1 + x)(1 + x^4)(1 + x^8 + x^{16})$	2	12
16	$(1 + x^4)$	$(1 + x)(1 + x^2)(1 + x^8 + x^{16})$	2	12

Table 3.2: Transmit and Receive Patterns for the sixteen designs obtained by factorizing the Virtual array Pattern

The 9 possible Tx and Rx designs from table 3.1 and 16 designs from table 3.2 will be analyzed based on their performance in a MIMO system and the best performing design will be selected.

By solving the convex optimization problem in equation 3.26, a virtual array will be synthesized for low sidelobes and using the General polynomial factorization method, the pattern of the virtual array will be factorized to obtain the Tx and Rx pattern which in turn will be used to determine the positions of the Tx and Rx antenna elements.

3.4. CONCLUSION

In this chapter two techniques are proposed for the design of non-uniform Tx and Rx arrays for interference suppression. The design techniques are based on the fact that lower the sidelobe level of the antenna in a certain direction, lower will be the power received from that direction i.e.both design techniques optimize the MIMO array for low sidelobes.

The thinning strategy chooses a topology, if the sidelobes of that topology are lower than a specified threshold, while the array is radiating towards the broadside direction. The pattern of the chosen topology is factorized using the polynomial factorization method to obtain the patterns of the Tx and Rx arrays.

The Multi beam optimization technique, changes the locations of the uniform array elements in such a way that the array will have low sidelobes while scanning at various angular directions, something the thinning technique does not take into account. The pattern of the designed MIMO virtual array is then factorized using the polynomial factorization method to obtain the Tx and Rx arrays.

The design techniques described in this chapter focus on optimizing the virtual array, rather than the physical Tx and Rx arrays, as all of the processing algorithms will be applied on the data obtained from the virtual array, it only makes sense to optimize it.

The Tx and Rx arrays obtained by the factorization of the virtual array pattern will be tested for a MIMO radar, for 500 realizations of a single target in the presence of the five interference sources at random locations. The SINR at the beamformer output derived in chapter 2 will be used as a metric of performance for the various designs.

4

RESULTS AND ANALYSIS

In the previous chapter, we discussed two techniques to design an antenna array with low sidelobes. In this chapter the aforementioned techniques in chapter 3 are implemented to design the Tx and Rx antenna array topologies, and the performance of these designs in a MIMO radar is checked by considering three cases with random positions of the target and interference sources, for each case the distance of the closest interference source from the target is changed i.e. when the closest interference source is 2° away from the target, 5° away from the target and 10° away from the target. The performance of the radar is checked for 500 simulations for each of the three cases.

4.1. ANTENNA ARRAY DESIGN

In this section the two techniques described in chapter 3 are implemented. The thinning strategy and the Multi beam optimization technique will only be used to design the MIMO virtual array, while the Polynomial Factorization method is used to factorize the pattern of the virtual array to obtain the Rx and Tx arrays.

4.1.1. THINNING STRATEGY

The thinning strategy is be used to design a MIMO array with 12 elements. For that purpose an aperture size of 16 elements is chosen and the threshold side lobe value SLL_{th} is chosen to be $-15dB$. With $K = 16$, $M = 2^{16} - 1$ on and off sequences are generated, and from these M sequences the ones with 12 no of on elements or the sequences with radiation efficiency of $12/16 = 0.75$ are selected. Within J, $H = \binom{12}{16} = 1820$ sequences only 617 belong to the set A as the PSL for these 617 sequences is below $PSL_{ula} = -13.2404dB$. Note that within J only those sequences are selected with PSL lower than PSL_{ula}, so the sequence with uniform spacing is not in set A.

Within A, only 5 sequences satisfy the condition of the SLL for the whole angular range $[-90,\ 90]$ excluding the main lobe, being lower than the predefined SLL_{th} of $-15dB$, and these 12 sequences are placed in the set Q. Within Q, all the sequences generate the same pattern. Any of the 5 topologies can be chosen as the final topology for

the virtual array, which will then be factorized via the polynomial factorization method to obtain the Tx and Rx pattern. Figure 4.1 show the radiation pattern of the chosen topology and figure 4.2 shows the antenna arrangements for the chosen topology.

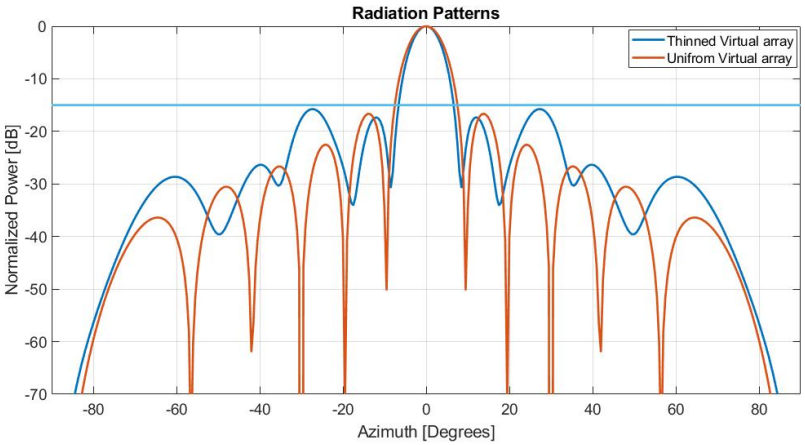

Figure 4.1: Comparison of Radiation Patterns for ULA and the Final topology obtained for a virtual array of 12 elements using the Thinning Strategy

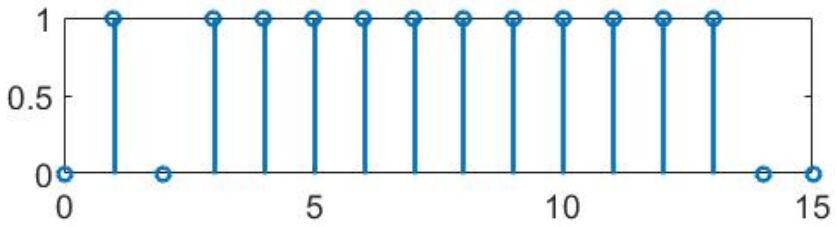

Figure 4.2: Antenna Arrangements for the Topologies for the virtual array of 12 elements. 1 indicates there is an antenna and 0 indicates the absence of the antenna

From figure 4.1, for the selected topology the PSL is less than the PSL_{ula} and the SLL is less than the predefined SLL_{th} of $-15dB$ for the whole angular range except the main lobe. From figure 4.2, the first and second elements are separated by λ and the rest elements are separated by $\lambda/2$. Due to the increased distance between the first and second element the effective aperture of the array has increased and we can see the effect of the increased aperture on the radiation pattern for the thinned virtual array in figure 4.1, the main lobe width of the thinned virtual array is smaller compared to the main lone width of the uniform virtual array. If for the topology the 11th and 12th array elements are separated by λ instead of the first and second element, the pattern of the array will remain the same. Note that the topologies are selected if the radiation patterns of the said topologies meet the bounds and rules set by the thinning algorithm, so if the bounds and rules of the thinning algorithm are changed we may end up with different topologies.

The Tx and Rx antenna positions can be obtained by factorizing the virtual array pattern in figure 4.1. Table 4.1 shows the nine possible designs obtained by factorizing the virtual array of 12 elements.

Design	$P_T(x)$	$P_R(x)$	N_T	N_R
1	$1+x$	$1+x^2+x^4+x^6+x^8+x^{10}$	2	6
2	$1+x^2$	$1+x+x^4+x^5+x^8+x^9$	2	6
3	$1+x^4+x^8$	$1+x+x^2+x^3$	3	4
4	$1+x$	$1+x^2+x^4+x^6+x^8+x^{10}$	2	6
5	$1+x^2+x^4$	$1+x+x^6+x^7$	3	4
6	$1+x^6$	$1+x^2+x^3+x^4+x^5+x^6$	2	6
7	$1+x+x^2$	$1+x^3+x^6+x^9$	3	4
8	$1+x^3$	$1+x+x^2+x^6+x^7+x^8$	2	6
9	$1+x^6$	$1+x+x^2+x^3+x^4+x^5$	2	6

Table 4.1: Transmit and Receive Patterns for the nine designs obtained by factorizing the Virtual array Pattern

The SINR performance of the nine possible Tx-Rx array designs shown in table 4.2 will be used to determine the best topology for MIMO processing, for that purpose each topology is tested with 500 simulations for a MIMO radar. For each simulation the topology is tested for single target in the presence of 5 interference sources. The power of the target signal is varied from -50dB to 50dB, and the power of the each of the interferes is 30dB. The receiver noise is set to be a zero mean, unit variance white Gaussian noise which is identical in each array element. The target and interference source positions are different for each simulation. Figure 4.3 shows the mean SINR for the nine topologies and figure 4.4 shows the CDF plot for the nine designs. There is no significant difference between the performance of the different designs, so any of the nine Tx and Rx pairs can be chosen.

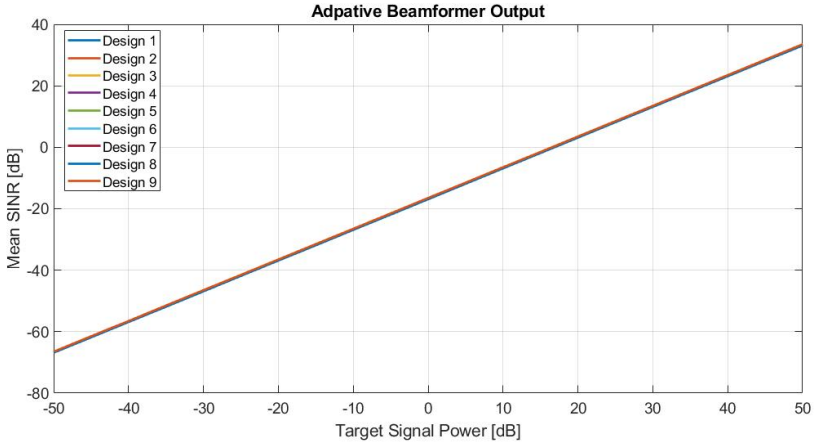

Figure 4.3: Mean output SINR of 500 simulations for different target and interference source positions for the nine Tx and Rx designs

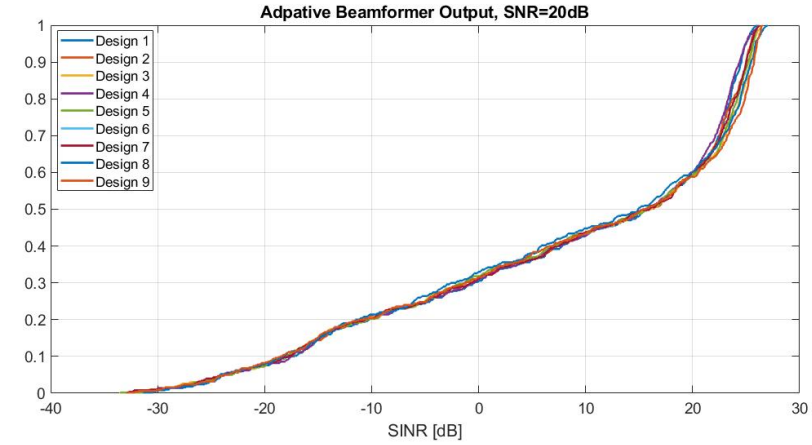

Figure 4.4: CDF plot of 500 simulations for different target and interference source positions for the nine Tx and Rx designs

The nine designs are based on factors of the virtual array pattern, and as MIMO processing is done on the virtual array, all designs in table 4.1 will create the same virtual array pattern, hence all the designs perform the same. For further investigation we will take design 3 and compare the performance of the MIMO radar for Uniform array and design 3.

For Design 3 the transmit pattern is $(1 + x^4 + x^8)$, the addition of 1^{st}, 5^{th} and 9^{th} terms of the virtual array pattern, So for the Tx array, the elements will be positioned in the same position of the 1^{st}, 5^{th} and 9^{th} elements of the virtual array. Same goes for the Rx array, the position of the Rx elements will be the positions of 1^{st}, 2^{nd}, 3^{rd} and 4^{th} elements of the virtual array. Figure 4.5 show the radiation patterns of the Tx and Rx arrays obtained by factorizing the thinned virtual array pattern in figure 4.1.

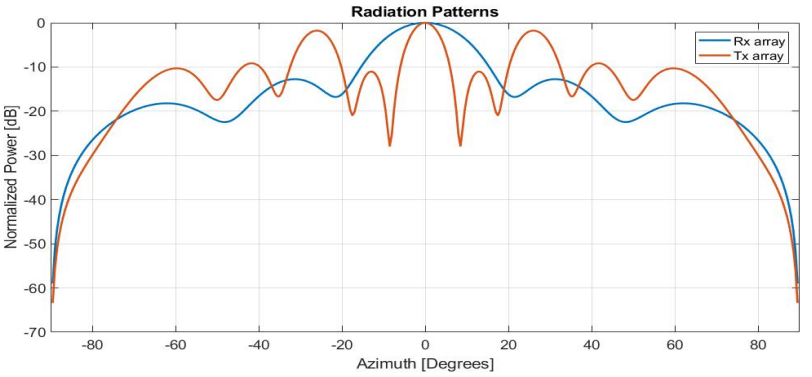

Figure 4.5: Tx and Rx radiation patterns obtained by factorizing the virtual array pattern

4.1.2. MULTI BEAM OPTIMIZATION TECHNIQUE

As discussed in chapter 3 The first step is to synthesize the virtual array via the optimization problem in equation 3.26. Using equation 3.26 two designs are considered, virtual array of 12 elements and virtual array of 24 elements. The pattern of the resulting arrays will then be factorized to obtain the patterns for Tx and Rx arrays, which in turn will be used to find the locations of the array elements in an x-y coordinate system.

MIMO VIRTUAL ARRAY OF 12 ELEMENTS

For the first we will optimize the positions of the virtual array of 12 elements for low sidelobes while scanning the main beam from +30 degree to -30 degree with 10 degree steps. For 12 elements $\theta_b = 10°$. The initial inter-element distance $d_{in} = 0.5\lambda$, and the minimum inter-elements distance is set to 0.1λ, this is chosen to allow more space for the movement of the elements. The maximum shift in position for each iteration is set to 0.16λ. Figure 4.6 shows the radiation patterns for different scan angles for multi beam optimization for 12 elements and figure 4.7 shoes the pattern of 12 element ULA.

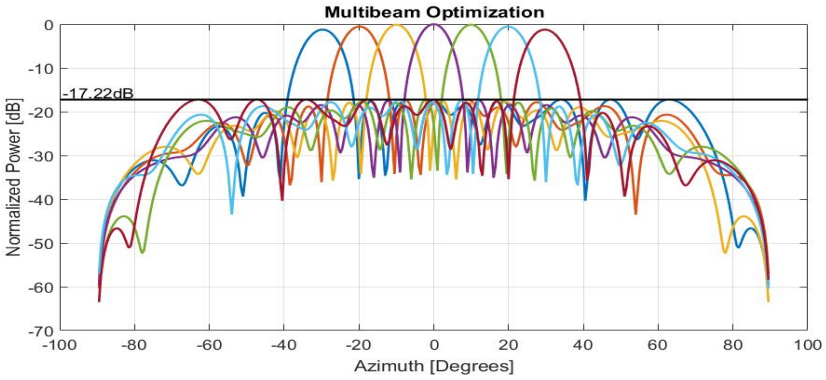

Figure 4.6: Pattern for Multiple beam optimization in ± 30 degrees ;
$\theta_b = 10 degrees, \mu = 0.16\lambda, d_{in} = 0.5\lambda, d_{min} = 0.1\lambda$

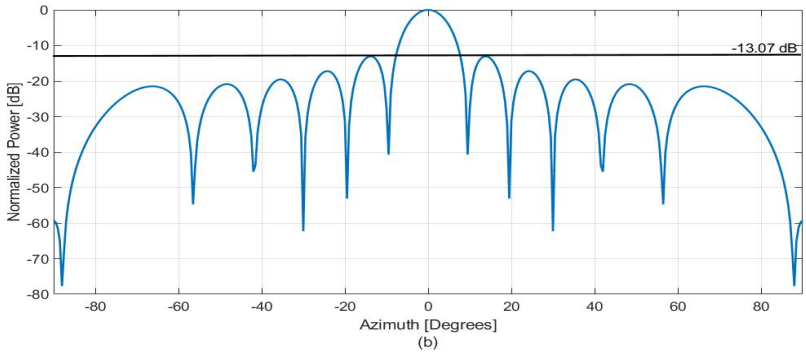

Figure 4.7: Pattern for ULA of 12 elements looking in broadside direction

In figure 4.6, it can be seen that for all scan angles the sidle lobe level for the optimized array is lower compared to the sidelobe level of the Uniform linear array of 12 elements looking at broadside direction in figure 4.7. Note that the patterns shown in figure 4.6 and 4.7 are the patterns for the virtual array, in other words these patterns are the product of the patterns of the Tx and Rx arrays. Table 4.2 shows the resulting optimal positions obtained by solving the convex optimization problem (equation 3.26) for the virtual array of 12 elements.

n	Pos/λ	n	Pos/λ
1	0.37925	7	3.9705
2	1.10335	8	4.6074
3	1.60645	9	4.75335
4	2.24335	10	5.0843
5	2.74335	11	5.9805
6	3.4674	12	6.6174

Table 4.2: Antenna Positions for 12 element non-uniform Virtual array

The nine possible Tx and Rx designs by factorizing the virtual array pattern of 12 elements in equation 3.43 are given again by table 4.1

The SINR performance of the nine possible Tx-Rx array designs shown in table 4.1 will be used to determine the best topology for MIMO processing, for that purpose each topology obtained by factorizing the virtual array pattern for the array in table 4.2 is tested with 500 simulations for a MIMO radar. For each simulation the topologies are tested for a single target in the presence of 5 interference sources. The power of the target signal is varied from -50dB to 50dB, and the power of the each of the interferes is 30dB. The receiver noise is set to be a zero mean, unit variance white Gaussian noise which is identical in each array element. The target and interference source positions are different for each simulation. Figure 4.8 shows the mean SINR for the nine topologies and figure 4.9 shows the CDF plot for the nine designs. There is no significant difference between the performance of the different designs, so any of the nine Tx and Rx pairs can be chosen.

As previously discussed, the nine designs are based on factors of the virtual array pattern, and as MIMO processing is done on the virtual array, all designs in table 4.1 will create the same virtual array pattern, hence all the designs perform the same. For further investigation we will take design 3 and compare the performance of the MIMO radar for Uniform array and design 3.

For Design 3 the transmit pattern is $(1 + x^4 + x^8)$, the addition of 1^{st}, 5^{th} and 9^{th} terms of the virtual array pattern, So for the Tx array, the elements will be positioned in the same position of the 1^{st}, 5^{th} and 9^{th} elements of the virtual array. Same goes for the Rx array, the position of the Rx elements will be the positions of 1^{st}, 2^{nd}, 3^{rd} and 4^{th} elements of the virtual array. The tables 4.3 and 4.4 show the position of the non-uniform Tx elements and Rx elements:

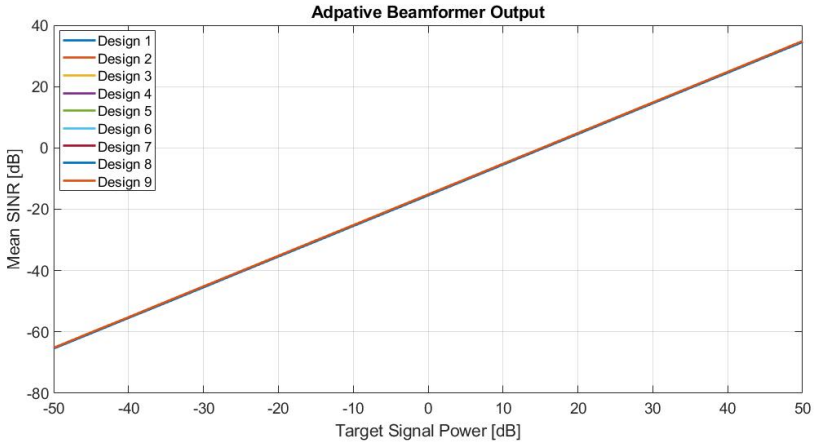

Figure 4.8: Mean output SINR of 500 simulations for different target and interference source positions for the nine Tx and Rx designs

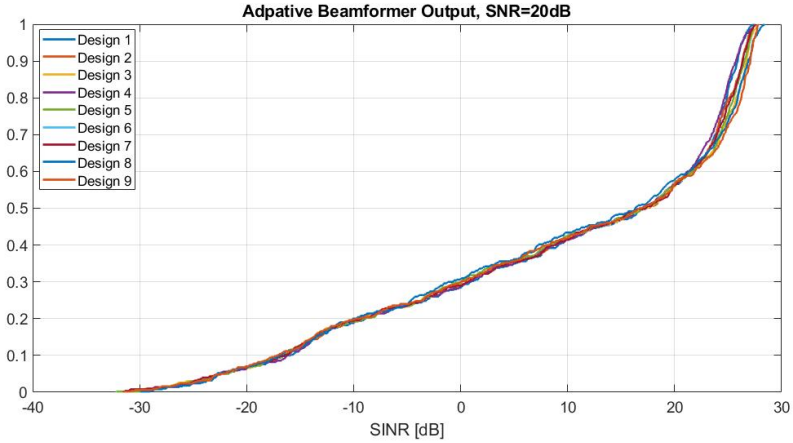

Figure 4.9: CDF plot of 500 simulations for different target and interference source positions for the nine Tx and Rx designs

n	Pos/λ
1	0.37925
2	2.74335
3	4.74335

Table 4.3: Tx array antenna positions

n	Pos/λ
1	0.37925
2	1.10335
3	1.60645
4	2.24335

Table 4.4: Rx array antenna positions

MIMO VIRTUAL ARRAY OF 24 ELEMENTS

For the second design we will optimize the positions of the virtual array of 24 elements for low sidelobes while scanning the main beam from +30 degree to –30 degree with 10 degree steps. The design steps are similar to the design for 12 elements previously discussed. For 24 elements $\theta_b = 5°$. The initial inter-element distance $d_{in} = 0.5\lambda$, and the minimum inter-elements distance is set to 0.1λ. The maximum shift in position for each iteration is set to 0.16λ. Figure 4.10 shows the radiation patterns for different scan angles for multi beam optimization for 12 elements and figure 4.11 shoes the pattern of 24 element ULA.

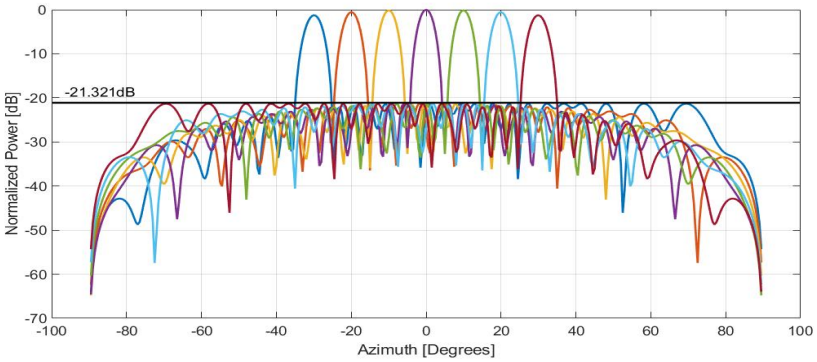

Figure 4.10: Pattern for Multiple beam optimization in ± 30 degrees ;
$\theta_b = 5degrees, \mu = 0.16\lambda, d_{in} = 0.5\lambda, d_{min} = 0.1\lambda$

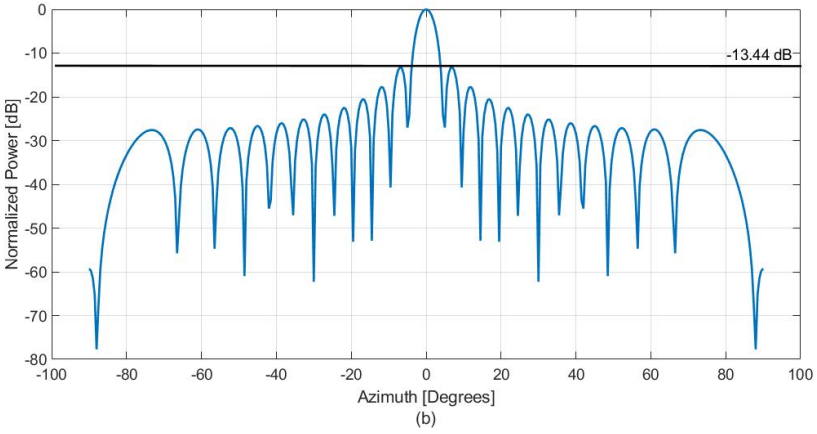

Figure 4.11: Pattern for ULA of 24 elements looking in broadside direction

Figure 4.10 shows a low sidelobe level for all the scan angles compared to figure 4.11 looking in the broadside direction, we compare the optimized patterns with the pattern of the ULA looking in broadside direction because the side lobe level for ULA will be the

lowest when the beam is in broadside. The patterns in the figures 4.10 and 4.11 are the patterns for the virtual array of 24 elements, i.e. they are the product of the Tx and Rx patterns. Table 4.5 shows the position of the resultant 24 element virtual array obtained by solving the optimization problem in equation 3.26.

n	Pos/λ	n	Pos/λ
1	-0.4385	13	6.3861
2	0.1750	14	6.7676
3	0.8289	15	7.1820
4	1.6343	16	7.6300
5	2.2159	17	8.1352
6	2.9070	18	8.7290
7	3.4727	19	9.2655
8	3.96837	20	9.8232
9	4.3575	21	10.3871
10	4.8191	22	11.3937
11	5.376	23	12.0407
12	5.9144	24	13.1992

Table 4.5: Antenna Positions for 24 element non-uniform Virtual array

The sixteen possible Tx and Rx designs by factorizing the virtual array pattern in equation 3.48 are given again by table 4.6

Design	$P_T(x)$	$P_R(x)$	N_T	N_R
1	$(1+x+x^2)$	$(1+x^3)(1+x^6)(1+x^{12})$	3	8
2	$(1+x^3)$	$(1+x+x^2)(1+x^6)(1+x^{12})$	2	12
3	$(1+x^6)$	$(1+x+x^2)(1+x^3)(1+x^{12})$	2	12
4	$(1+x^{12})$	$(1+x+x^2)(1+x^3)(1+x^6)$	2	12
5	$(1+x+x^2)$	$(1+x^3)(1+x^6)(1+x^{12})$	3	8
6	$(1+x^3)$	$(1+x+x^2)(1+x^6)(1+x^{12})$	2	12
7	$(1+x^6)$	$(1+x+x^2)(1+x^3)(1+x^{12})$	2	12
8	$(1+x^{12})$	$(1+x+x^2)(1+x^3)(1+x^6)$	2	12
9	$(1+x^4+x^8)$	$(1+x)(1+x^2)(1+x^{12})$	3	8
10	$(1+x)$	$(1+x^2)(1+x^4+x^8)(1+x^{12})$	2	12
11	$(1+x^2)$	$(1+x)(1+x^4+x^8)(1+x^{12})$	2	12
12	$(1+x^{12})$	$(1+x)(1+x^2)(1+x^4+x^8)$	2	12
13	$(1+x^8+x^{16})$	$(1+x)(1+x^2)(1+x^4)$	3	8
14	$(1+x)$	$(1+x^2)(1+x^4)(1+x^8+x^{16})$	2	12
15	$(1+x^2)$	$(1+x)(1+x^4)(1+x^8+x^{16})$	2	12
16	$(1+x^4)$	$(1+x)(1+x^2)(1+x^8+x^{16})$	2	12

Table 4.6: Transmit and Receive Patterns for the sixteen designs obtained by factorizing the Virtual array Pattern

As the processing will be done on the virtual array and all the designs in table 4.6 will generate the same virtual array the performance of the 16 designs will be the same, we saw a similar behaviour in design for MIMO array of 12 elements, so any of the 16 designs can be chosen. For further investigation we will choose Design 13 and compare the performance of the MIMO radar for Uniform array and design 13.

For design 13 the Tx pattern is $(1 + x^8 + x^{16})$, the addition of $1^{st}, 9^{th}$ and 17^{th} term of the virtual array pattern. The positions of the Tx elements will be the same as the positions of the $1^{st}, 9^{th}$ and 17^{th} elements of the virtual array. Same goes for the Rx array, the position of the Rx elements will be the positions of $1^{st}, 2^{nd}, 3^{rd}, 4^{th}, 5^{th}, 6^{th}, 7^{th}$ and 8^{th} elements of the virtual array. The tables 4.7 and 4.8 show the position of the Tx elements and Rx elements:

4

n	Pos/λ
1	-0.4385
2	4.3575
3	8.1325

Table 4.7: Tx array antenna positions

n	Pos/λ
1	-0.4385
2	0.1750
3	0.8289
4	1.6343
5	2.2159
6	2.9070
7	3.4727
8	3.9837

Table 4.8: Rx array antenna positions

4.2. PERFORMANCE

As mentioned before the performance of the proposed array designs in the previous section will be checked based on the SINR at the output of the adaptive beamformer discussed in chapter 2. The simulation environment is set as such, we will consider three cases with random position of the target and interference sources, for each case the distance of the closest interference source from the target is changed i.e. when the closest interference source is 2° away from the target, 5° away from the target and 10° away from the target. 500 simulations are done for each of the cases and the performance is ranked based on the average SINR for the 500 simulations. For each simulation the topology is tested for single target in the presence of 5 interference sources. The power of the target signal at the receiver is varied from -50dB to 50dB, and the power of the each of the interference sources at the receiver is 30dB. The receiver noise is set to be a zero mean, unit variance white Gaussian noise which is identical in each array element.

4.2.1. THINNING STRATEGY

As explained in the previous section, the thinning strategy is used to design the virtual array, The pattern of the virtual array is factorized to obtain the Tx and Rx patterns and antenna positions. The MIMO model and the adaptive beamformer described in chapter 2 are implemented along with the final array topology via the thinning strategy, on MATLAB. Figures 4.12 shows the mean SINR performance for the topology for the three

cases. Figure 4.13 compares the MIMO performance of the topology via thinning with the ULA.

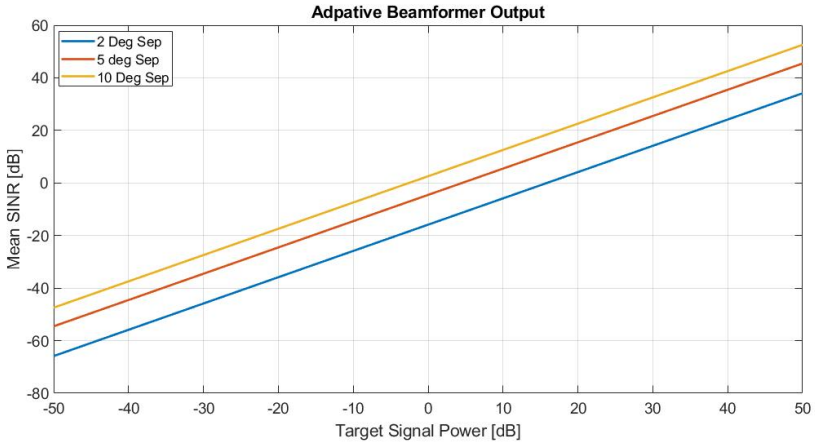

Figure 4.12: Average Output SINR of 500 simulations for 2,5 and 10 Degree separation of the target and the closest interference source for array obtained via the thinning strategy

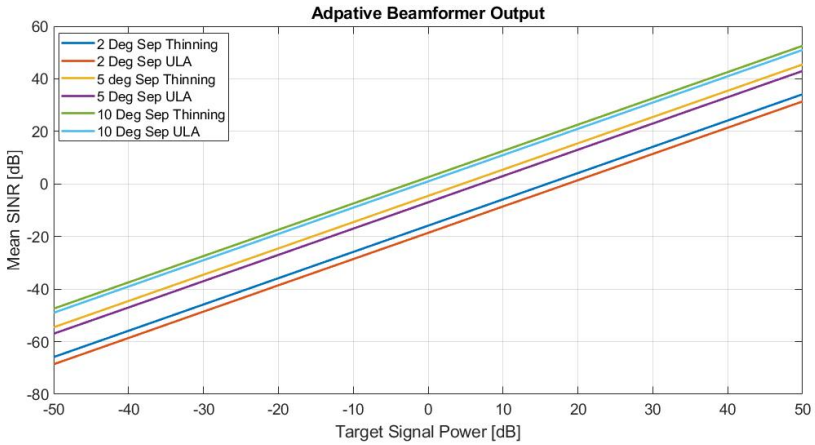

Figure 4.13: Comparison of average Output SINR of 500 simulations for 2,5 and 10 Degree separation of the target and the closest interference source for the Antenna array design via the Thinning Strategy with ULA

From figure 4.12, we can see improvement in the average output SINR as the interference sources are more spread out. In figure 4.13, for the closest interference source 2° away from the target, the average SINR improves by 2.75 dB, for the case of closest interference source 5° away from the target, the average SINR improves by 2.45 dB, for the case of closest interference source 10° away from the target, the average SINR improves by 1.58 dB. In figure 4.13 we see that as the closest interference source moves

away from the target the gain in the performance decreases, indicating an improved rejection of main lobe interference for the new designed topology. This can be explained with the fact that for the new topologies the aperture of the array is bigger than that of the uniform linear array of 12 elements, which will cause the beam to be narrow, hence improving the main lobe performance of the radar.

4.2.2. MULTI BEAM OPTIMIZATION TECHNIQUE

Same simulation scenarios are used for analyzing the MIMO performance of the designed Tx and Rx array for the 12-element virtual array and 24 element virtual array via the Multi beam optimization technique and polynomial factorization method. As discussed in the previous section, for 12 elements virtual array, a design with 3 elements for the Tx array and 4 elements for the Rx array is chosen, and for 24 elements a design with 3 elements for the Tx array and 8 elements for the Rx array is chosen.

MIMO VIRTUAL ARRAY OF 12 ELEMENTS

The MIMO model and the adaptive beamformer from chapter 2 and the Tx and Rx array topologies from tables 4.3 and 4.4 are implemented in MATLAB. Figure 4.14 shows the mean SINR performance of the designed array for 500 simulations of different target and interference source positions. In figure 4.15 the SINR performance of the designed array is compared with the performance of the uniform linear arrays of 3 transmitters and 4 receivers for the three simulation scenarios. Figure 4.16 is the CDF plots for the data shown in figure 4.16.

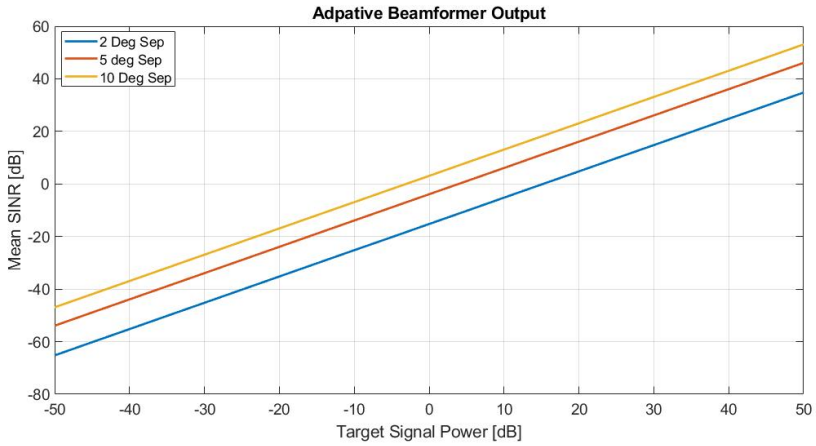

Figure 4.14: Average Output SINR of 500 simulations for 2,5 and 10 Degree separation of the target and the closest interference source for 3 element Tx array and 4 element Rx array design via Convex Optimization and Polynomial Factorization

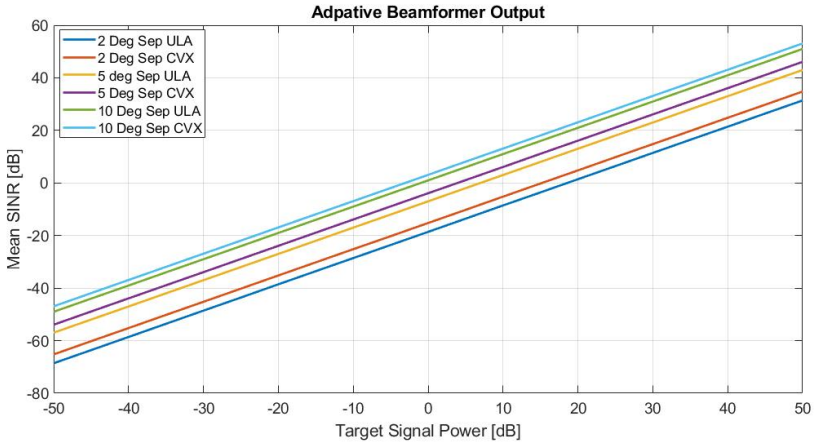

Figure 4.15: Comparison of average Output SINR of 500 simulations for 2,5 and 10 Degree separation of the target and the closest interference source for 3 element Tx array and 4 element Rx array design via Convex Optimization and Polynomial Factorization with ULA

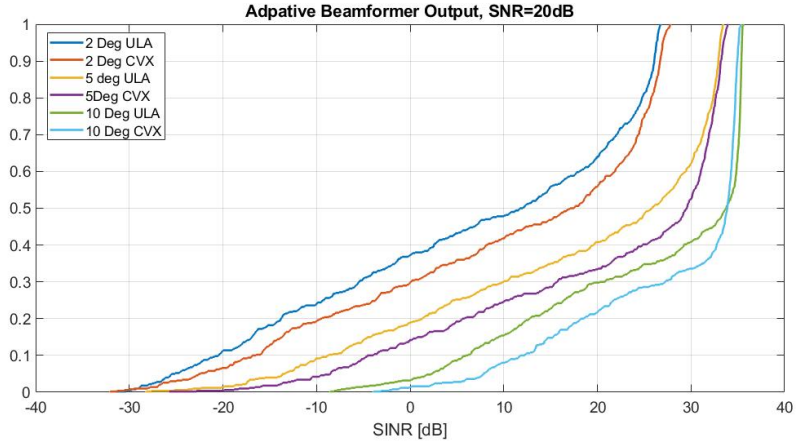

Figure 4.16: Comparison of CDF plots of 500 simulations for 2,5 and 10 Degree separation of the target and the closest interference source for 3 element Tx array and 4 element Rx array design via Convex Optimization and Polynomial Factorization with ULA

From figure 4.15, We can see clear improvement in the performance of the radar, and when the interference sources are much closer to the target, the performance increase is higher than when the interference sources are more spread out. Observe figure 4.15, for the closest interference source 2° away from the target, the average SINR improves by 3.35 dB, for the case of closest interference source 5° away from the target, the average SINR improves by 3.09 dB and for the case of closest interference source 10° away from the target, the average SINR improves by 2.13 dB. The same improvement in the performance can be seen in the CDF plots in figure 4.16, for the case of closest inter-

ference source 2° away from the target, the CDF curves for the designed topology and the ULA are more separated compared to the other two cases. The low SINR part of the curve represent the cases for which the remaining four interference sources are closer to the closest interference source. From the CDF curves we can see that in very noisy conditions the designed non-uniform array topology has better performance than the uniform array. Figure 4.17 compares the performance of the array designed via the thinning strategy and the multi beam optimization technique.

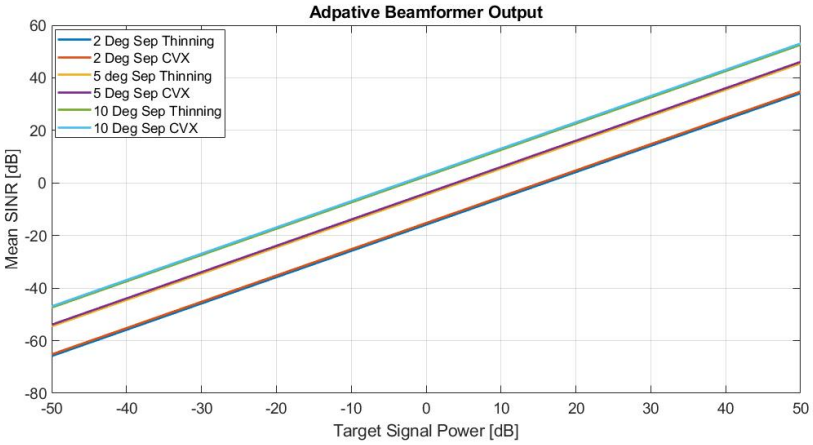

Figure 4.17: Comparison of average Output SINR of 500 simulations for 2,5 and 10 Degree separation of the target and the closest interference source for the Antenna array designed via the Thinning Strategy with ULA

The array designed via the optimization technique outperforms the array via thinning strategy by about 0.6dB for all the three cases. This can be explained by the fact that the array designed via the optimization technique will enjoy low sidelobes even as the main beam is scanned, but the array via thinning was chosen for low sidelobes when the main beam was looking in the broadside direction, so it may not have the same sidelobe performance if the main beam is scanned at various directions

MIMO VIRTUAL ARRAY OF 24 ELEMENTS

Tables 4.7 and 4.8 for the Tx and Rx array elements position and the MIMO model and the adaptive beamformer are implemented in MATLAB. Figures 4.18 shows the mean SINR performance of the designed array for 500 simulations for the three cases. In figure 4.19 the SINR performance of the designed array is compared with the performance of the uniform linear arrays of 3 transmitters and 8 receivers for the three simulation scenarios. Figure 4.20 is the CDF plots for the 500 simulations of the three cases with the comparison of the proposed design with the ULA.

Observe figure 4.19, for when the closest interference source is 2° away from the target, the average SINR improves by 2.29 dB, for the case of closest interference source 5° away from the target, the average SINR improves by 1.69 dB and for the case of closest interference source 10° away from the target, the average SINR improves by 0.95 dB. We can see that when the interference sources are much closer to the target, the per-

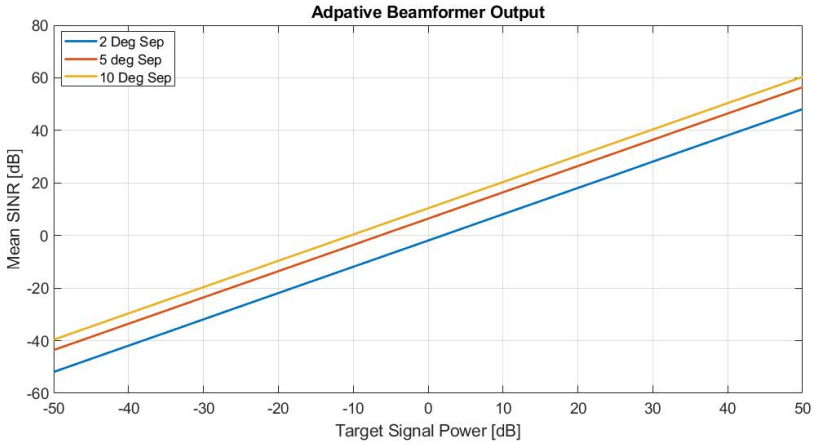

Figure 4.18: Average Output SINR of 500 simulations for 2,5 and 10 Degree separation of the target and the closest interference source for 3 element Tx array and 8 element Rx array design via Convex Optimization and Polynomial Factorization

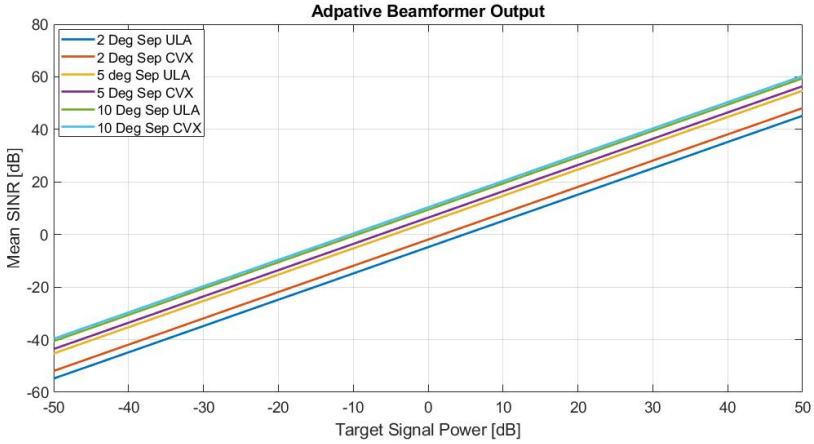

Figure 4.19: Comparison of average Output SINR of 500 simulations for 2,5 and 10 Degree separation of the target and the closest interference source for 3 element Tx array and 8 element Rx array design via Convex Optimization and Polynomial Factorization with ULA

formance increase is higher than when the interference sources are more spread out, similar behaviour is observed in figure 4.15 for 12 element virtual array. For figure 4.19 the performance gain is less compared to in figure 4.15, this can be explained using the main beam width of the virtual array, for 24 elements the main beam is 5 degrees thinner than the main beam for 12 elements. This makes the suppression of the interference source close to the targets for the adaptive beamformer easy for 24 elements compared to 12 elements, indicating that the bigger the aperture of the virtual array the better will be its performance.

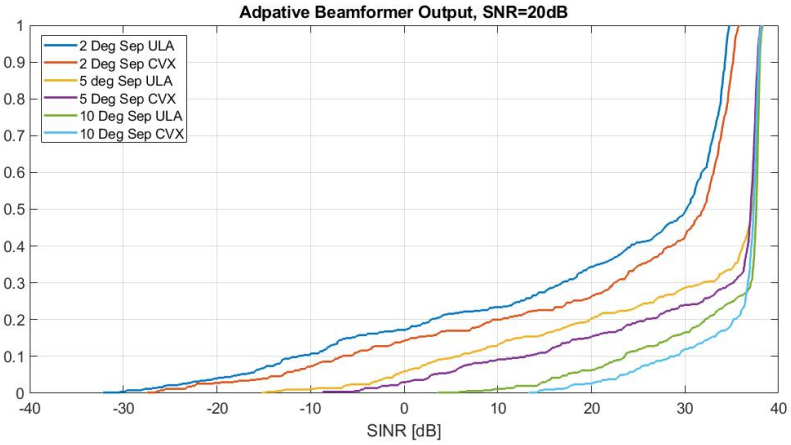

Figure 4.20: Comparison of CDF plots of 500 simulations for 2,5 and 10 Degree separation of the target and the closest interference source for 3 element Tx array and 8 element Rx array design via Convex Optimization and Polynomial Factorization with ULA

From figure 4.20, the CDF plots for the designs are spread out at low SINR values and are overlapping at high SINR values, the low SINR part of the curve represent the cases for which the remaining four interference sources are closer to the closest interference source and as the sources spread out from the closest source, the curves for the ULA and the designed array overlap, indicating the performance of the designed array is better when the interference sources are close to the target, than the ULA.

4.3. ANALYSIS

In the previous section we saw that the topologies designed via thinning strategy and convex optimization and factorization method had a higher gain in performance in noisy conditions compared to less noisy conditions, as seen in figure 4.13,4.15 and 4.19. We can explain this phenomenon using the beam patterns of the MIMO virtual array. Consider a target at 10° and five interferes at [7°,30°,40°,-30°,-10°]. Note that the angle of the first interference source is 3° away from the angle of the target. Figure 4.21 shows the beam patterns of the 12 element virtual array for the designed topologies and the pattern for the virtual array for uniformly spaced Tx and Rx arrays after suppression is applied.

From figure 4.21 we can see that the main beam after suppression for the array designed via multi beam optimization is much narrower than the uniform linear array, and the main beam maxima for the virtual array via multi beam optimization(CVX) is much closer to the position of the target than the main beam for uniform linear array, due to this reason more power is received from the target after suppression for Non-uniform array compared to ULA, hence improving the output SINR of the beamformer. Figure 4.22 compares the output SINR for non-uniform array and ULA for different separation of the closest interference source from the target. We can see that the improvement in performance of the non-uniform MIMO array is much higher when the separation of the closest interference source and the target is small. From figure 4.22, when the separation

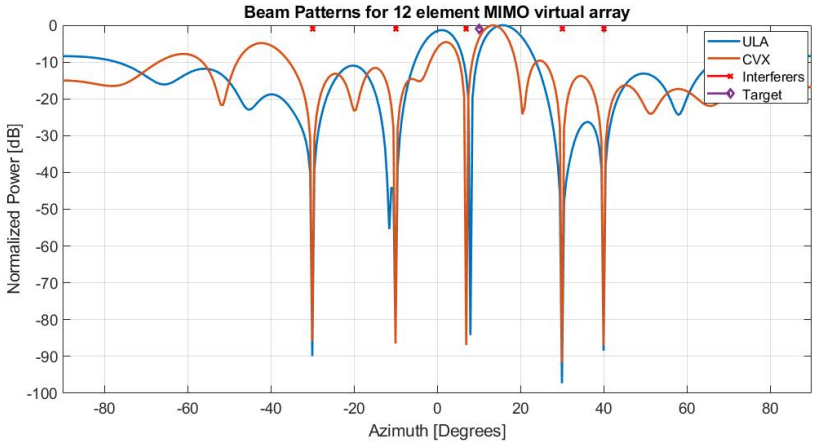

Figure 4.21: Beam pattern comparison of non-uniform MIMO array (CVX) and Uniform MIMO array (ULA) after suppression for target at 10° and five interference sources at [7°,30°,40°,-30°,-10°]

is 2°, the non-uniform MIMO array outperforms the uniform MIMO array by 1.87dB. For a separation of 3°, the non-uniform MIMO array outperforms the uniform MIMO array by 1.81dB. This trend continues for when the target and the interference source are separated by 4°,5° and 6°, where the SINR improves by 1.15dB,1dB and 0.33dB. From this behaviour of the non-uniform MIMO array, it can be inferred that the proposed non-uniform MIMO array design via multi beam optimization and polynomial factorization enhances the main lobe interference rejection capabilities of the array compared to uniform MIMO array. Similar behaviour will be observed for the non-uniform MIMO array of 24 elements.

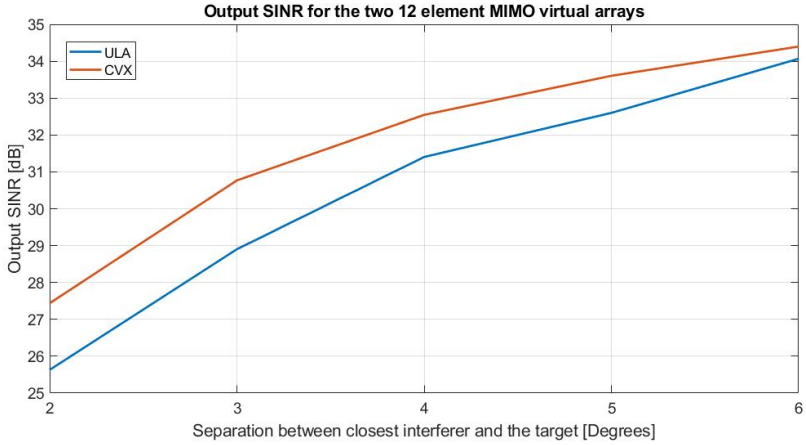

Figure 4.22: Comparison between the Output SINR for non-uniform MIMO array (CVX) and Uniform MIMO array (ULA)

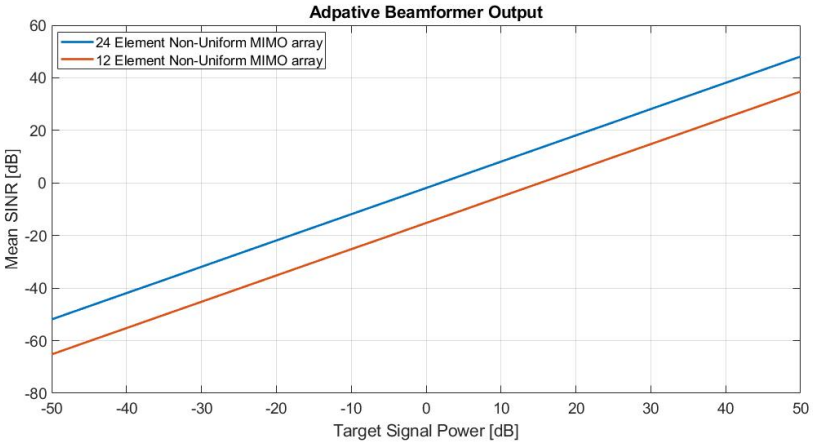

Figure 4.23: Average output SINR of 500 simulations with a single target and 5 interference sources with the closest source separated from the target by 2 degrees, for 24 and 12 element Non-Uniform MIMO arrays

Figure 4.23 compares the mean SINR for 12 element and 24 element virtual array. We can see a significant improvement in the performance of the MIMO system with 24 elements, indicating that the larger the aperture of the virtual array the smaller will be the main beam of the virtual array and better will be performance after suppression. Figure 4.23 can explain the difference in performance gain between figures 4.15 and 4.19. As the aperture of the virtual array increases, the beamwidth reduces. The reduction in beamwidth will make the suppression of the interference sources close to the target easier compared to the MIMO array with large beamwidth, hence we observe an improvement of 16.7dB in the output SINR for 24 element Non-uniform MIMO array compared to the 12 element Non-uniform MIMO array.

4.4. CONCLUSION

In this chapter the design techniques described in chapter 3 are implemented. A virtual array of 12 elements with sidelobes less than a threshold of $-15dB$ is designed using the thinning strategy. By using the polynomial factorization method, the Tx and Rx array patterns are obtained by factorizing the virtual array pattern, which in turn give the antenna arrangement for the Tx and Rx arrays. The performance of the Tx and Rx arrays in a MIMO system is tested for 500 realizations of a single target in the presence of 5 interference sources, when the closest interference source to the target is 2°, 5° and 10° away. The non-uniform Tx and Rx arrays result in an improvement of the average SINR by 2.75dB for 2° separation, 2.45dB for 5° separation and 1.58dB for 10° separation of the target and the closest interference source.

The multi beam optimization techniques designs a virtual array which has low sidelobes even when scanning the main beam, something the thinning strategy does not take into account. Virtual arrays of 12 and 24 elements are designed using the multi beam optimization technique and factorized. The factors of the virtual array are tested

for a MIMO system for 500 realizations of a single target in the presence of 5 interference sources, when the closest interference source to the target is 2°, 5° and 10° away.

The 12 element non-uniform array yields an improvement of the average SINR by 3.35dB for 2° separation, 3.09dB for 5° separation and 2.13dB for 10° separation of the target and the closest interference source. The higher average SINR for the arrays designed via the multi beam optimization is due to the arrays having low sidelobes compared to the arrays via the thinning strategy.

The 24 element non-uniform array yields an improvement of the average SINR by 2.29dB for 2° separation, 1.69dB for 5° separation and 1dB for 10° separation of the target and the closest interference source. The reduction in the SINR gain for when the closest interference source moves away from the target is due to the fact that the designed non-uniform arrays have a larger aperture compared to their uniform counterpart. The larger aperture gives the array narrower main lobe width, which helps the adaptive beamformer in suppressing an interference source very close to the target more effectively.

The lower improvement of the average SINR for 24 elements compared to 12 elements is also due to increased aperture of the virtual array . The increased aperture of the virtual array makes the job of suppressing an interference source very close to the target easier. So the uniform array is already pretty effective in suppressing the interference sources, so the reduced aperture of the non-uniform array for 24 elements will not have the same impact on the MIMO system as that in the case of a MIMO system with 12 elements.

The antenna arrangements from tables 4.3 and 4.4 for a virtual array of 12 elements will be used in the next chapter to model an automotive radar with a non-uniform MIMO antenna array to verify that the non-uniform array performs better even if the effects of mutual coupling, antenna and dielectric losses are taken into account.

5

CST MODELLING AND SIMULATION

Planar antennas due to their low cost, lower profile and ease of integration with other systems are common components in sensing systems and applications They can also be used at high frequencies such as at 77GHz for automotive applications. Also new ultra-wideband communication systems rely on planar antennas due to their unique properties [32]. One unique properties of the planar arrays is that they can form arrays by combining very simple elements like micro strip patches, they can also from phased and conformal arrays. Keeping these properties in mind, one can conclude that planar antennas are a good choice for building front ends for mm-wave applications for sensing, radar and communication systems. In this chapter the elements for the Tx and Rx arrays are modelled in CST. Using the array topologies form chapter 4, the Tx and Rx arrays are formed with the designed elements. A radar scenario of a single target at 1 meters in the background of 5 interferes is simulated, and MATLAB is used for forming of virtual array and beamforming. The output SINR at the beamformer is measured and compared with the results obtained in chapter 4.

5.1. SINGLE ANTENNA DESIGN

For automotive applications, an antenna is required that radiates in the broadside direction i.e. does not have an omnidirectional pattern similar to the pattern of a half-wavelength dipole. A patch antenna is a good choice for this as the radiation properties of a patch antenna are of broadside nature due to the fringing fields present between the patch and the ground plane. Figure 5.1 and 5.2 show a micro strip patch and the azimuth radiation pattern for the patch.

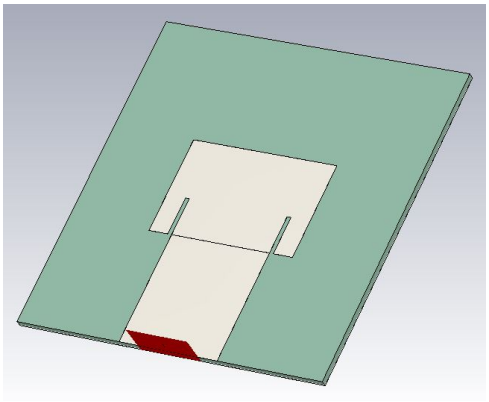

Figure 5.1: Patch antenna

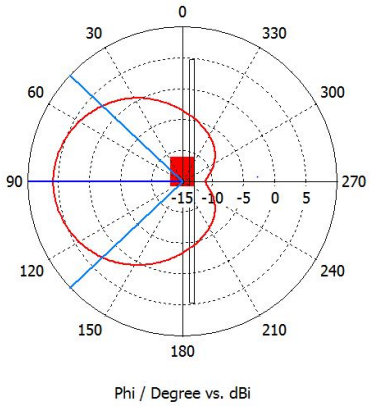

Figure 5.2: Azimuth radiation pattern for the patch antenna

From figure 5.2 it can be seen that the patch antenna radiates in the broadside direction, hence fulfilling the requirement for being chosen as the primary element for an automotive radar antenna.

5.1.1. SINGLE PATCH ELEMENT

A single patch to be used in the Tx and Rx array of the automotive radar is designed and simulated here. The substrate chosen for the patch is the 5 mil Ro3003 with the thickness of 0.13mm which results in the permittivity of 3±0.04. As the automotive radars usually operate at 77GHz, the patch model is tuned to resonate at the 77GHz. The rectangular patch has a length of 1.078mm and a width of 1mm. The rectangular patch is fed with a microstrip line of width 77μm, to avoid the spurious radiation of the line, the impedance of the microstrip is designed to be 100Ohms. Figure 5.3 shows the designed microstrip patch and figure 5.4 shows the reflection coefficient for the patch. we can see from figure 5.4 that the patch resonates at the required frequency.

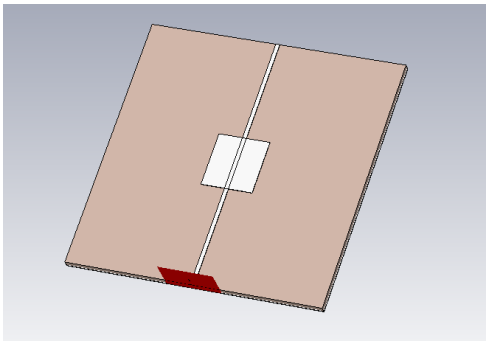

Figure 5.3: Single Patch cell

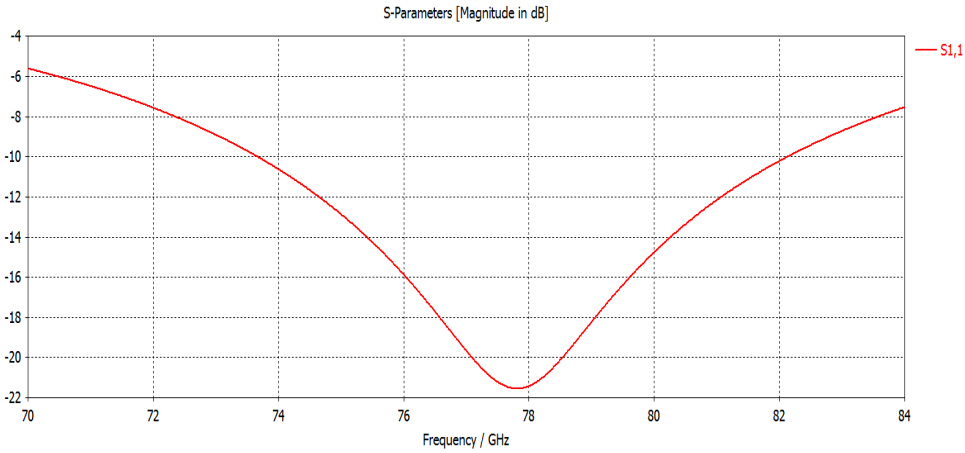

Figure 5.4: Single Patch cell

In figure 5.5 we see the elevation and azimuth radiation pattern for the designed single patch element. It can be observed that although the azimuth radiation is acceptable, the elevation beam is too broad for effective sensing in automotive applications, as the broad beam is not suitable for accurate sensing and will undermine the function of the radar.

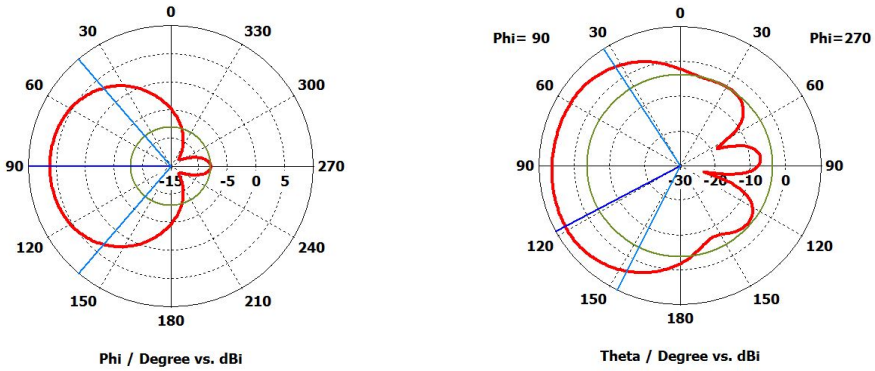

(a) Azimuth pattern

(b) Elevation pattern

Figure 5.5: Azimuth and elevation patterns for the single patch element

5

5.1.2. PATCH COLUMN

The radiation properties of the antenna in the elevation plane can be improved by increasing the aperture of the patch. This can be achieved by using patch columns instead of single patches [32] i.e. the length of the patch is increased resulting in a narrow elevation beam. The length of the antenna is increased by connecting 8 patch cells through a microstrip line. The distance between two consecutive patches is adjusted to get a phase shift of 360 degrees between the input edges of the patches, doing this will cause the main beam to point in the broadside direction [32]. Figure 5.6 shows the patches arranged in a column connected with each other through the microstrip line. All the patches in the column are of the same size, the length of the patches is 1.078 mm and the width is 1mm, the distance between the patches is 2.818mm which is chosen to achieve phase shift of 360 degrees between input edges of the patches at the resonance frequency of 77GHz.

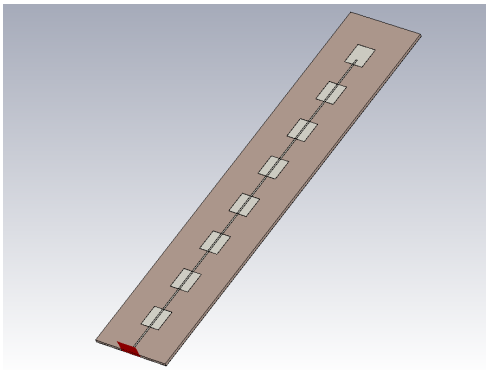

Figure 5.6: Patch column

The substrate chosen for this design is the 5 mil Ro3003 with the thickness of 0.13mm.

Figures 5.7 and 5.8 shows the elevation and azimuth patterns for the patch column. From 5.7 we can see that by increasing the length of the antenna element, the elevation beam is much narrower, and the antenna radiates in the broadside direction for the azimuth and elevation planes.

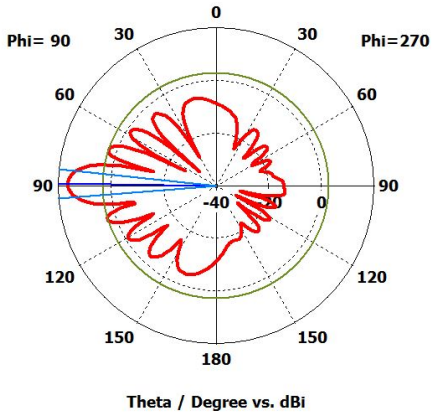

Figure 5.7: Elevation Pattern for the Patch column

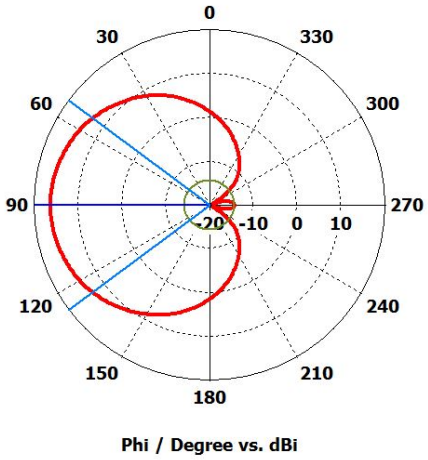

Figure 5.8: Azimuth Pattern for the Patch column

Even though the narrow beam in figure 5.7 will improve the radar sensing function, the sidelobes in the elevation pattern can lead to ground clutter which in turn will affect the measurement efficiency of the radar. Lowering the sidelobes is beneficial for reducing the ground clutter, for that purpose a simple method is to vary the widths of the patches in the column [32]. Based on the approach in [32], the widths of the patches are varied. The variation of the widths of the patches will not affect the radiation pattern

of the antenna but will only reduce the sidelobe level.

Figure 5.9 shows the new array element with varying patch widths. The length of all the patches is the same i.e. 1.078mm. The width of Patch 1 is 0.4366mm, Patch 2 is 0.655mm, Patch 3 is 0.873mm and of Patch 4 is 1.078mm, and the same widths of Patch 1 to 4 are used for Patch 5 to Patch 8 but in descending order. The distance between patches is 2.818mm to achieve phase shift of 360 degrees between input edges of the patches at the resonance frequency of 77GHz. Figure 5.10 shows the elevation patterns for the same widths and varying widths. We can see that the sidelobe level indeed is reduced from -13.3dB for same widths to -18.7dB for varying widths. An improvement of 5.4dB is achieved by varying the widths of the patches.

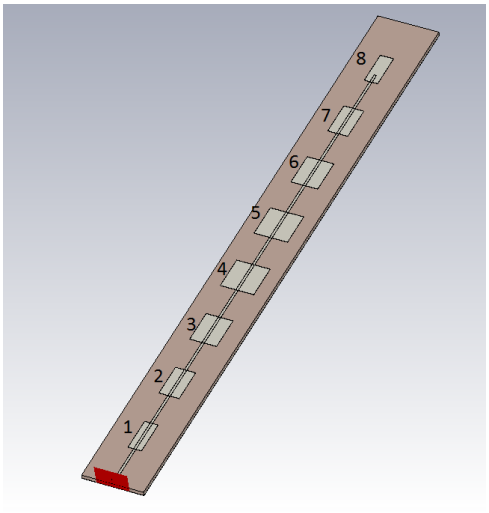

Figure 5.9: Patch column with varying patch widths

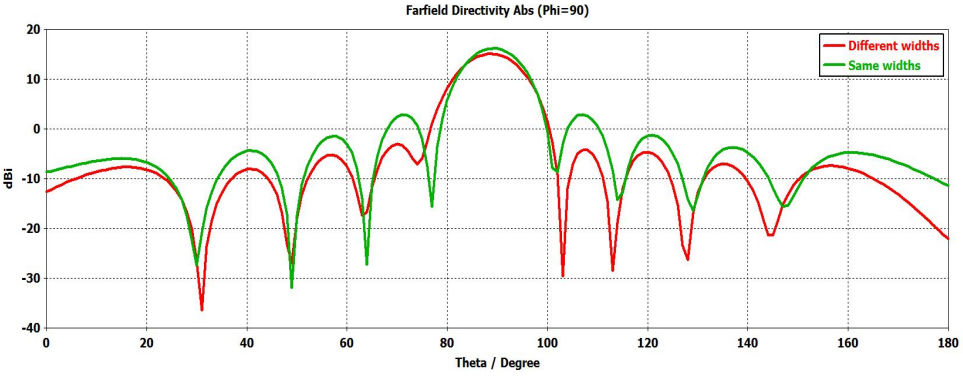

Figure 5.10: Comparison of Elevation Patterns

Results of matching show that by increasing the length of the antenna and varying

the widths, the antenna still resonates at 77GHz which is necessary for a radar that will operate at that frequency. Figure 5.11 shows the return loss for the patch column antenna with varying patch widths.

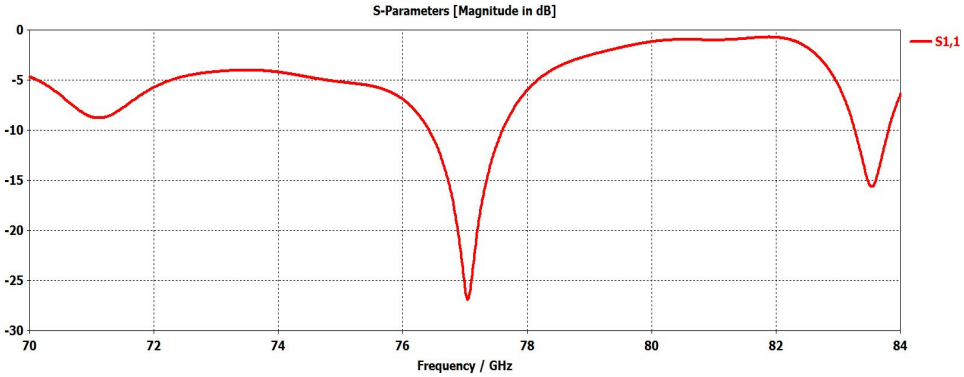

Figure 5.11: Return loss of the patch column with varying widths

Using the above discussed antenna, the Tx and Rx will be designed. For the uniform array The Tx array will have three antennas separated by $2\lambda = 7.78mm$ and the Rx array will have four closely spaced antenna arrays separated by $\lambda/2 = 1.945mm$. And for the arrays obtained by factorizing the virtual array pattern obtained in tables 4.3 and 4.4, the first and second element of the Tx array will be separated by 2.36λ, the second and third will be separated by 2λ, and for the Rx the separation between first and second is 0.724λ, second and third is 0.503λ, third and fourth is 0.636λ. The arrays will operate at the resonance frequency of 77GHz.

5.2. TRANSMITTER ARRAY DESIGN

5.2.1. UNIFORM ARRAY

For the uniformly spaced array the inter-element distance for the Tx array is $2\lambda = 7.78mm$. Figure 5.12 gives a closer look at the Tx array of 3 elements.

As the elements of the Tx array are spaced out, the effect of mutual coupling will be lower compared to a dense array. Figure 5.13 shows the s-parameters for the three Tx channels when the Tx channels are excited individually.

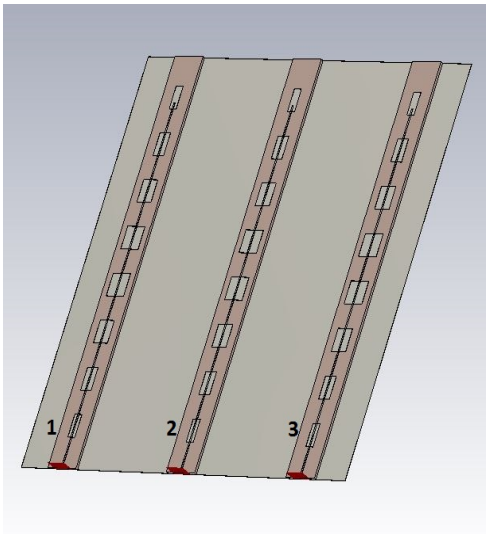

Figure 5.12: The Uniform Tx Array

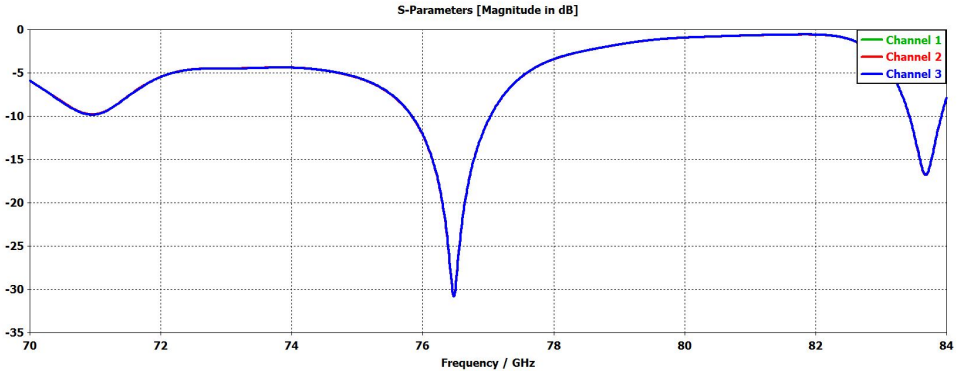

Figure 5.13: Passive S-Parameters of Tx Channels

By exciting the elements individually we will observe the reflection coefficients for each element or each Tx channel. As one channel is excited the value of reflection coefficient in other channels will be the measure of how much the excited channel will impact the other Tx channels. Figures 5.14-5.16 show the reflection coefficients in the other two channels when one of the three Tx channels is excited. From figure 5.14, when channel 1 is excited the coupling due to channel 1 on channel 2 is higher as channel 1 and channel 2 are immediate neighbours compared to the coupling on channel 3 due to channel 1. From figure 5.15 coupling due to channel 2 on channel 1 and channel 3 is same as channel 1 and 3 are separated by equal distance from channel 2. From figure 5.16, we see higher coupling on channel 2 compared to channel 1, as channel 3 is closer to channel 2.

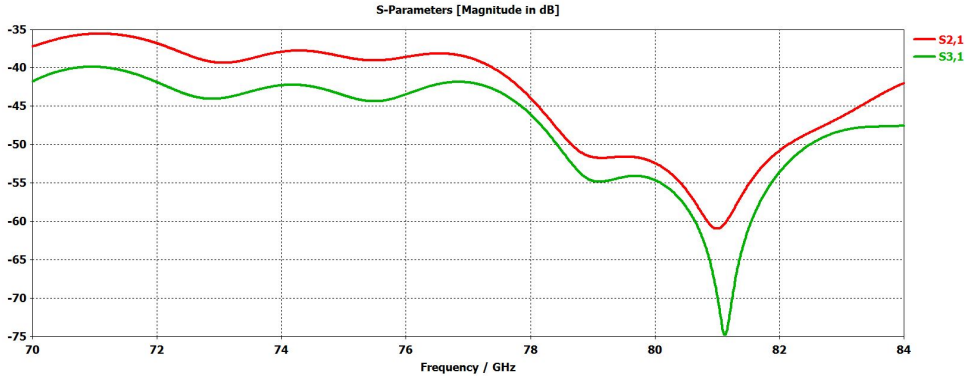

Figure 5.14: Mutual Coupling (Channel 1 Excited)

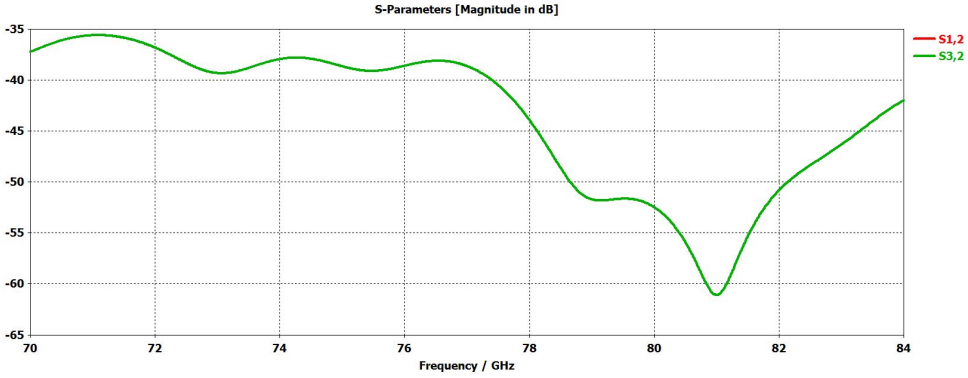

Figure 5.15: Mutual Coupling (Channel 2 Excited)

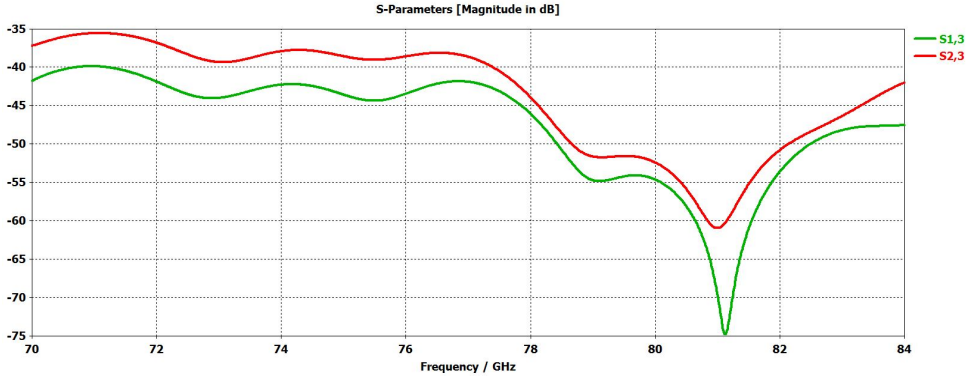

Figure 5.16: Mutual Coupling (Channel 3 Excited)

By exciting all the Tx channels simultaneously, we can include the mutual coupling seen in figures 5.14-5.16 and calculate the active S-parameters of the three Tx channels. Figure 5.17 shows the active s-parameters of the Tx channels. As the Tx elements are spread out, the mutual coupling will not have a major impact on the performance of the Tx elements. This is clear in figure 5.17, as the active s-parameters of the three Tx channels are similar.

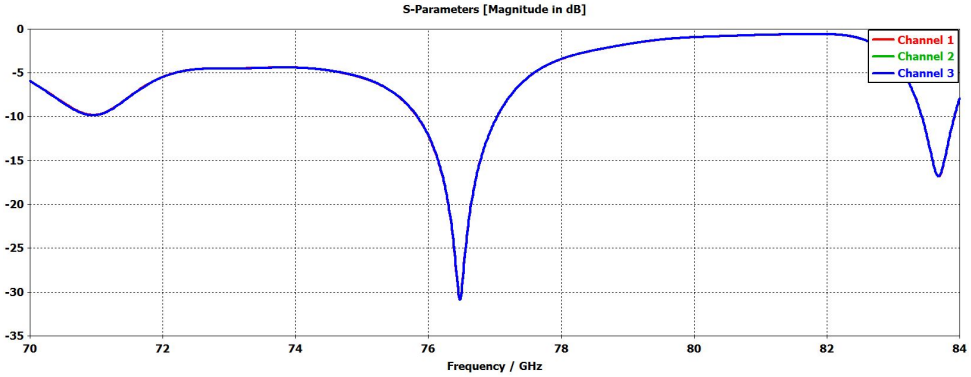

Figure 5.17: Active S-Parameters for the Three Tx channels

5.2.2. NON-UNIFORM ARRAY

From table 4.3 , for the non-uniform Tx array, the first and second element of the Tx array will be separated by 2.36λ, the second and third will be separated by 2λ at 77GHz. Figure 5.18 gives a closer look at the non-uniform Tx array.

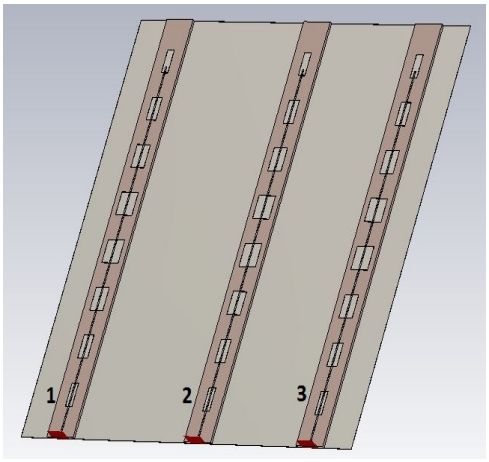

Figure 5.18: Non-Uniform Tx Array

As the first element is more further away compared to the uniform array, the mutual

coupling between the first channel and the other two channels will be lower compared to the uniform array. Figures 5.19-5.21 show the reflection coefficients in the other two channels when one of the three Tx channels is excited. From figure 5.19, when channel 1 is excited the coupling due to channel 1 on channel 2 is higher as channel 1 and channel 2 are immediate neighbours compared to the coupling on channel 3 due to channel 1. From figure 5.20 coupling due to channel 2 on channel 1 is slightly less compared to coupling of channel 1 on 3, as channel 1 and channel 2 are separated by 2.36λ and channel 2 and 3 are separated by 2λ at 77GHz. From figure 5.21, we see higher coupling on channel 2 compared to channel 1, as channel 3 is closer to channel 2.

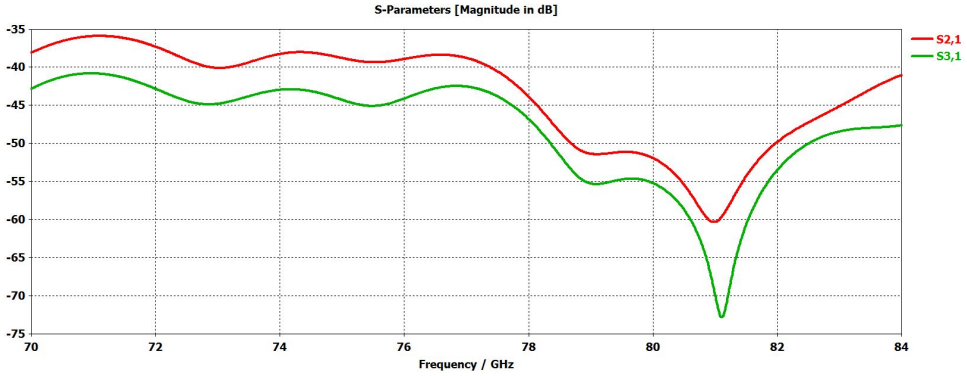

Figure 5.19: Mutual Coupling (Channel 1 Excited)

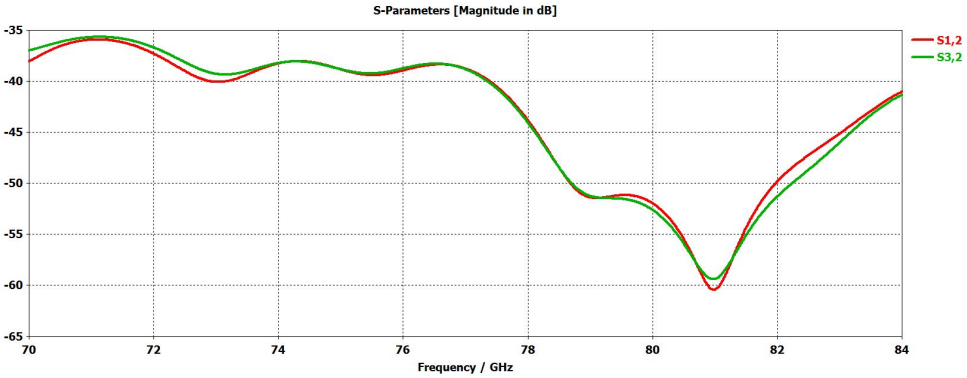

Figure 5.20: Mutual Coupling (Channel 2 Excited)

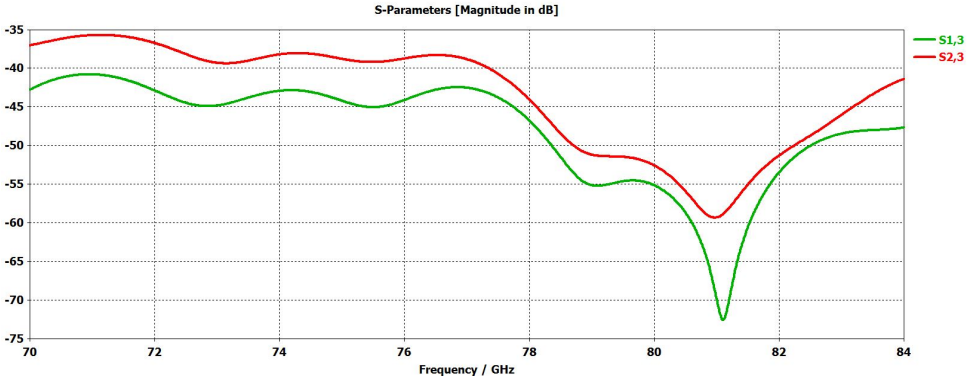

Figure 5.21: Mutual Coupling (Channel 3 Excited)

Since one element (channel 1) of the non-uniform Tx array is more separated from other elements (channel 2 and 3) compared to the uniform Tx array, the coupling effect on channel 1 due to channel 2 and 3 will be lower compared to the case of uniform Tx array. Figures 5.22 and 5.23 show the mutual coupling on channel 1 when channel 2 and 3 are excited for uniform and non- uniform Tx array.

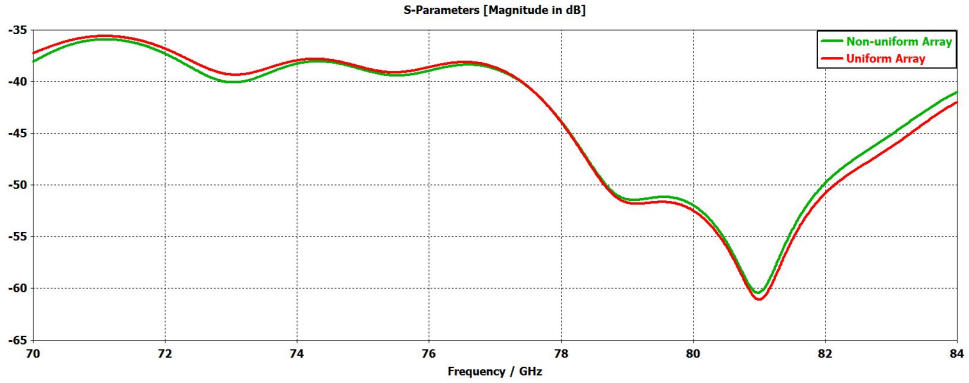

Figure 5.22: Mutual Coupling on channel 1 for uniform and non-uniform Tx Array (Channel 2 excited)

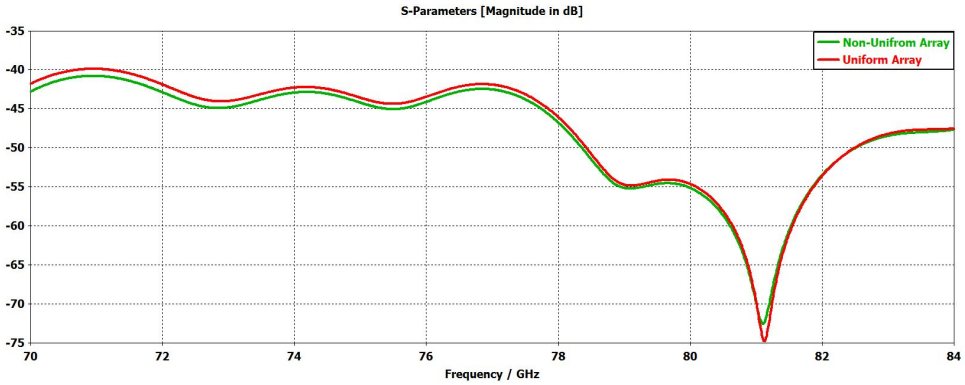

Figure 5.23: Mutual Coupling on channel 1 for uniform and non-uniform Tx Array (Channel 3 excited)

As the first channel is only moved by 0.36λ from its position in the uniform Tx array, in figures 5.22 and 5.23 we see a slight reduction in the affect of the mutual coupling due to channel 2 and 3 on channel 1. Hence the non-uniform Tx array is slightly better performing compared to the uniform linear array.

5.3. RECEIVER ARRAY DESIGN

5.3.1. UNIFORM ARRAY

For the uniformly spaced array the inter-element distance for the Rx array is $\lambda/2 = 1.945mm$. The Rx array consists of four elements or channels. Figure 5.24 gives a closer look to the uniformly spaced Rx array.

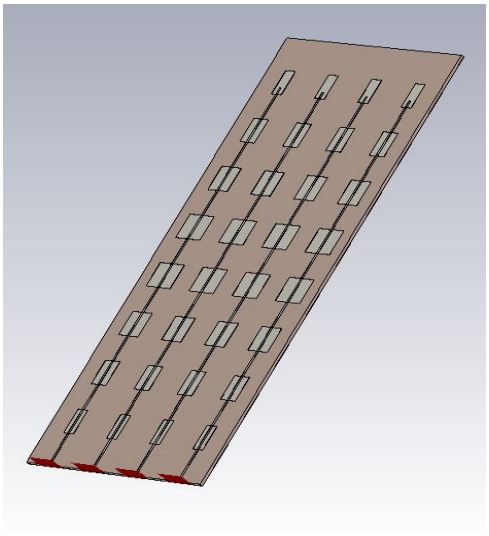

Figure 5.24: The Uniform Rx Array

Due to closely spaced elements, the affect of mutual coupling between the Rx elements will be more prominent compared to the widely spaced Tx array. Figure 5.25 shows the s-parameters for the four Rx channels when the Rx channels are excited individually.

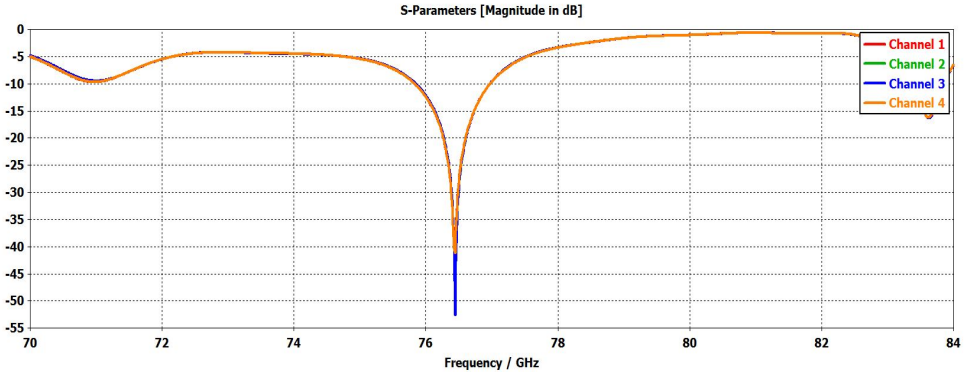

Figure 5.25: Passive S-Parameters of the four Rx channels

By individually exciting the channels we can see as how much affect the excited channel will have on the other channels. Figures 5.26-5.29 illustrate the mutual coupling of the neighbouring antennas/channels on each antenna/channel. From figure 5.26 we can see that, mutual coupling between the immediate neighbours, 2nd channel and the 1st channel is high compared to the coupling between the 1st and the rest of the receiver channels (3 and 4). In figure 5.27, the immediate neighbours 1 and 3 will have strong effect compared to the coupling between 4 and 2. The coupling will have a strong influence due to channel 2 and channel 4 compared to one between channel 1 and 3, as seen in figure 5.28. Channel 3 being the closer element will have a strong coupling affect with channel 4 compared to channel 1 and 2, as seen in figure 5.29.

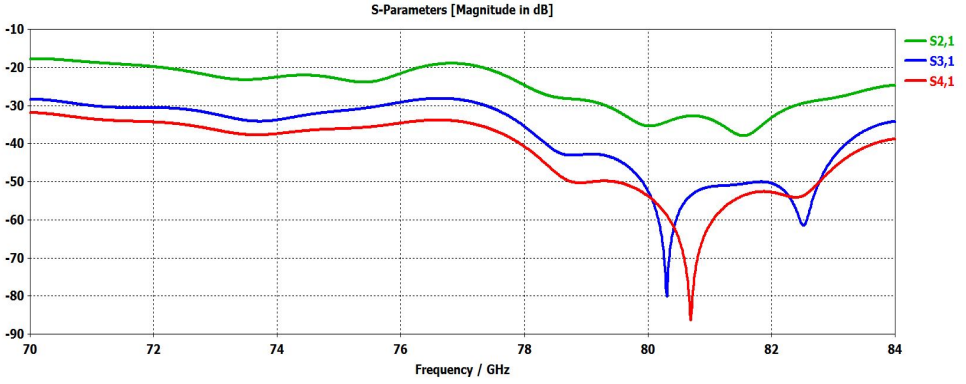

Figure 5.26: Mutual Coupling (Channel 1 excited)

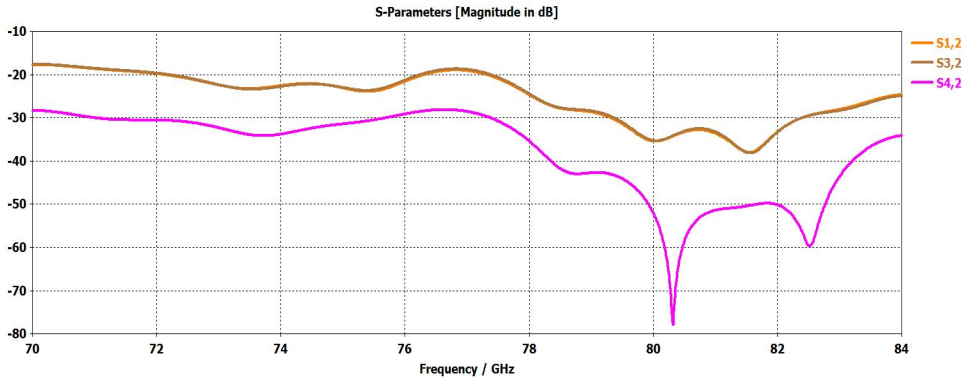

Figure 5.27: Mutual Coupling (Channel 2 excited)

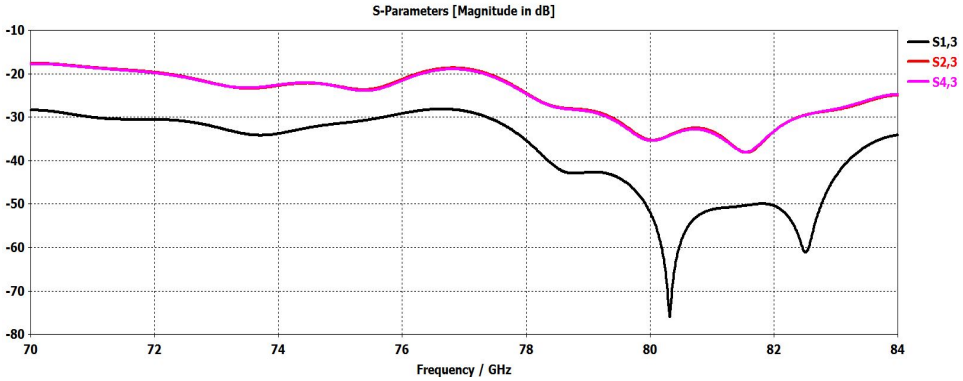

Figure 5.28: Mutual Coupling (Channel 3 excited)

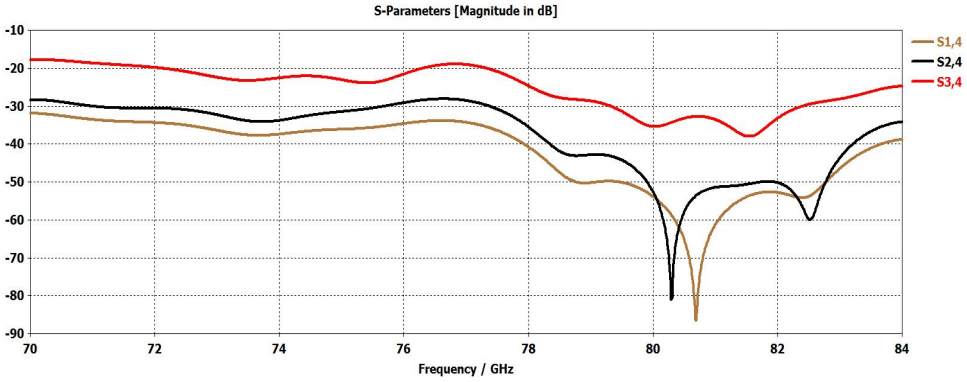

Figure 5.29: Mutual Coupling (Channel 4 excited)

By exciting all the Rx channels simultaneously, we can include the mutual coupling seen in figures 5.26-5.29 and calculate the active S-parameters of the four Rx channels. Figure 5.30 shows the active s-parameters of the Rx channels. From the figure it is clear that the performance of the four channels has degraded due to mutual coupling. Being the centre elements the affect of coupling is strongest on channel 2 and channel 3, causing higher degradation in the performance of the these channels compared to the side elements (channel 1 and 4).

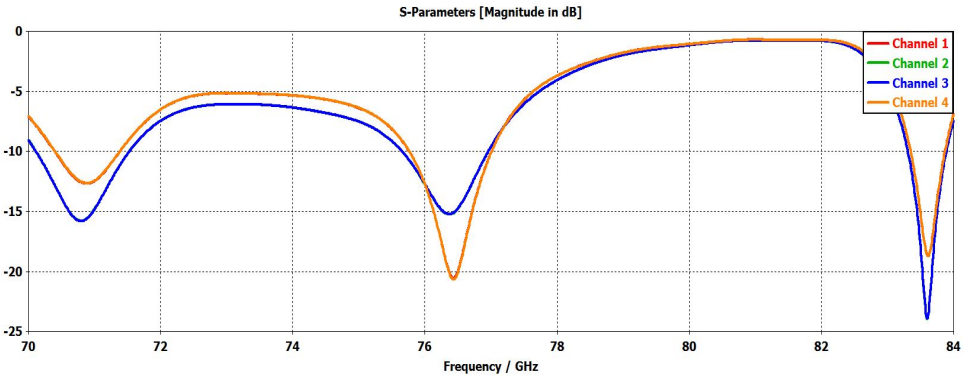

Figure 5.30: Active S-Parameters of the four Rx channels

5.3.2. NON-UNIFORM ARRAY

From table 4.4 , for the Rx array, the separation between first and second is 0.724λ, second and third is 0.503λ, third and fourth is 0.636λ. The arrays will operate at the resonance frequency of 77GHz. Figure 5.31 gives a closer look at the non-uniform Rx array.

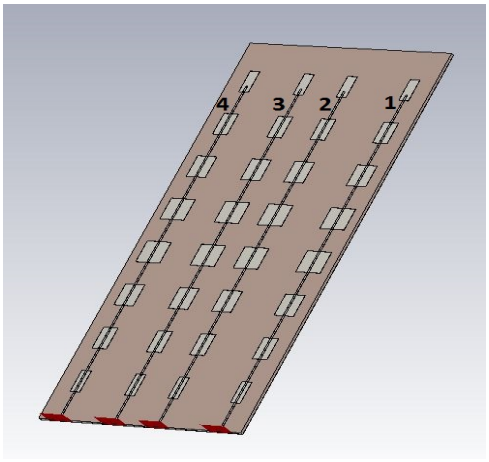

Figure 5.31: The Non-Uniform Rx Array

As the elements in the non-uniform array are more spaced out compared to the uniform array, the mutual coupling between the Rx elements will be lower. Using the similar approach as for the case of uniform Rx array, we can see the mutual coupling due to each channel on the neighbouring channels. Figures 5.32-5.35 illustrate the mutual coupling between the Rx channels. Taking a closer look at figures 5.33 and 5.34, we see the improvement for the non-uniform array. From figure 5.33, we can see that coupling between 1st and 2nd channel is lower than the coupling between 2nd and 3rd channel, and if we recall for the uniform array (figure 5.27), the coupling for 1st and 3rd channel were equal as the 1st and 3rd element were equidistant from the 2nd element, by moving the 1st element at a distance of 0.724λ from the 2nd element, the 3rd element is much closer to the 2nd element than the 1st, hence we can see the reduction of coupling affect on the 1st element than the 3rd element. Same can be said for figure 5.34, the 4th element is much more farther from the 3rd element than the 2nd element, hence we can see a reduction in the coupling affect on the 4th channel compared to the 2nd channel.

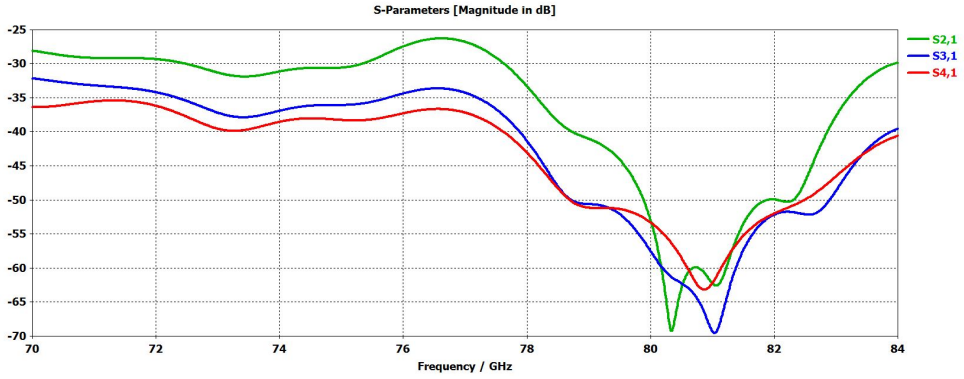

Figure 5.32: Mutual Coupling (Channel 1 excited)

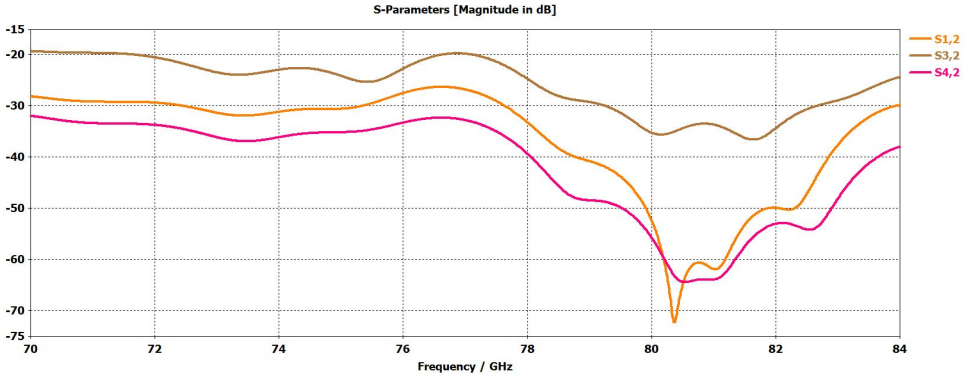

Figure 5.33: Mutual Coupling (Channel 2 excited)

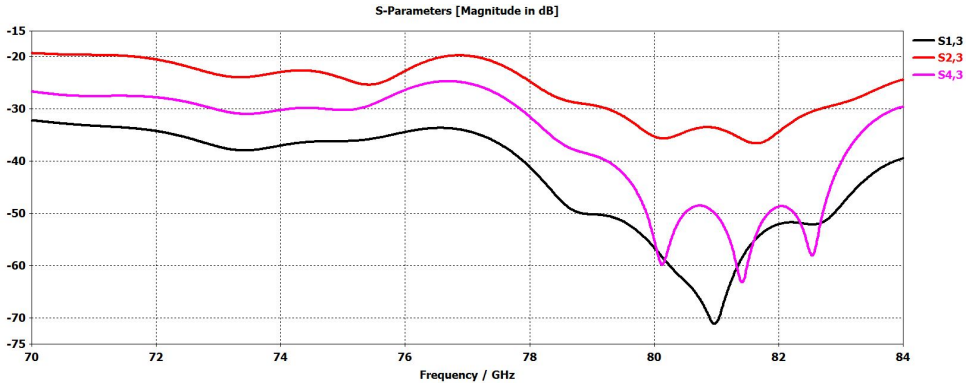

Figure 5.34: Mutual Coupling (Channel 3 excited)

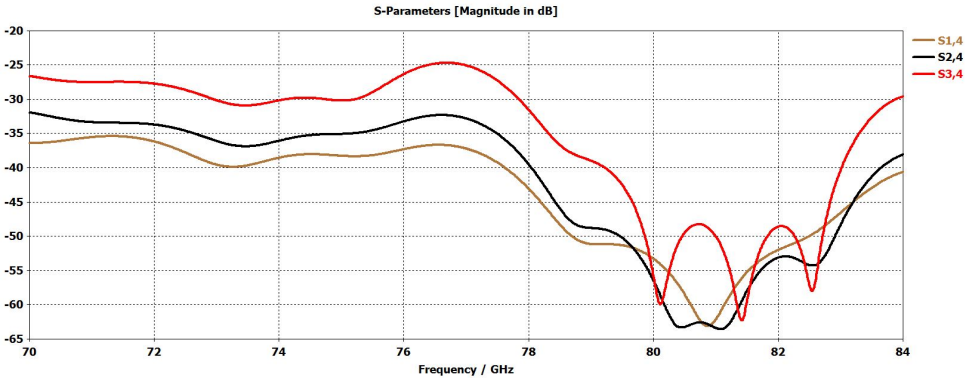

Figure 5.35: Mutual Coupling (Channel 4 excited)

By exciting all the Rx channels simultaneously, we can include the mutual coupling seen in figures 5.32-5.35 and calculate the active S-parameters of the four Rx channels. Figure 5.36 shows the active s-parameters of the Rx channels. As in the case of non-uniform array, the 1st element and the 4th element are moved further apart from the 2nd and 3rd element of the array, an improvement in the active s-parameter for the 1st and 4th channel can be seen. This indicates that as the 1st element is moved further away from the 2nd element the affect of mutual coupling on the 1st element due to the 2nd element is reduced and same is the case for 4th and 3rd element. Figure 5.37 shows the mutual coupling due to the 2nd channel on the first channel for uniform and non-uniform arrays, and figure 5.38 shows the mutual coupling due to 3rd channel on the 4th channel. From figure 5.37, as the distance between the 1st and 2nd element is 0.724λ, for the 1st channel the mutual coupling drops by 6.94dB for the non-uniform array compared to the uniform array at resonance, and from figure 5.38, at resonance the mutual coupling for the 4th channel drops by 5.45dB for the non-uniform array. The coupling for the 4th channel is higher than the 1st channel because the distance between the 1st and 2nd element is higher than the distance between the 4th and 3rd element, so the

affect of the neighbouring elements on the 1st element will be lower compared to the affect on 4th element. By keeping the above comparison in mind, it can be concluded that the non-uniform array will be performing better than its uniform counterpart.

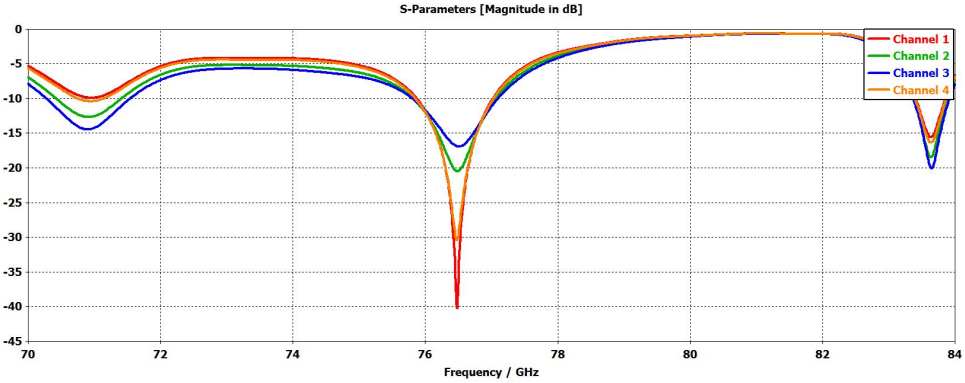

Figure 5.36: Active S-parameters for non-uniform Rx array

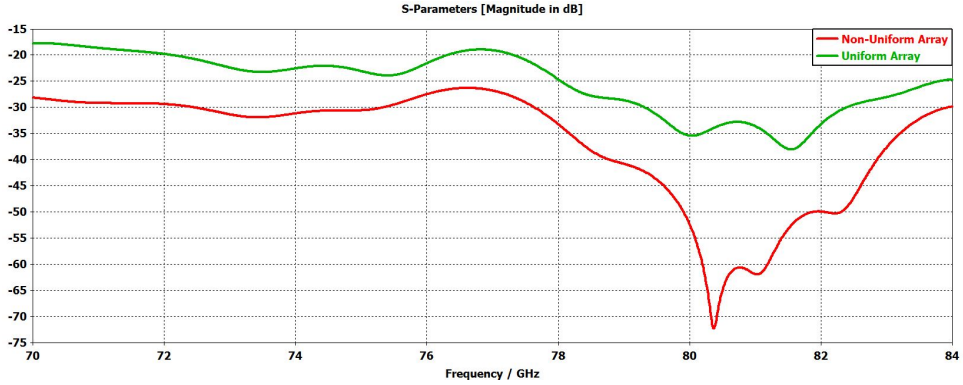

Figure 5.37: Mutual coupling on 1st channel due to 2nd channel

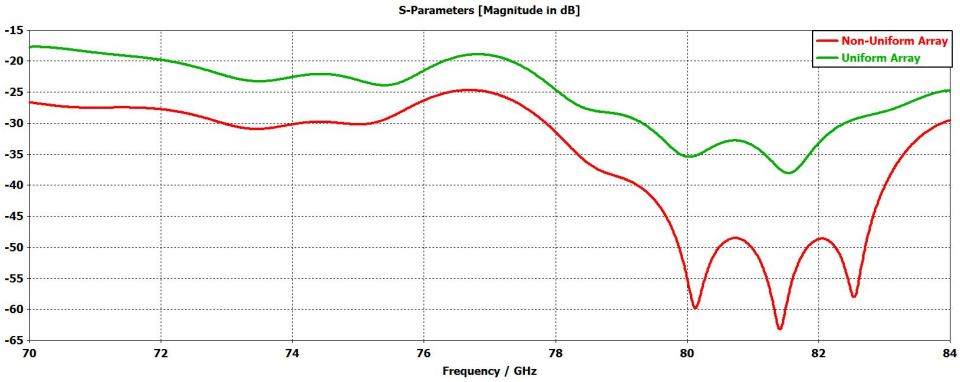

Figure 5.38: Mutual coupling on 4th channel due to 3rd channel

5

5.4. MIMO ARRAY DESIGN AND PERFORMANCE

5.4.1. MIMO ARRAY

Using the designed Tx and Rx array, a radar transceiver can be designed. Antenna diversity can be realized by placing the Tx and Rx antennas in the same plane separated by some distance. By employing antenna diversity, the quality and reliability of the radar system can be improved. Keeping that in mind, both the Tx and Rx antennas are placed along the horizontal axis (y-axis) separated by a distance of 2λ. The distance of 2λ is chosen so that the interference between the Tx and Rx array elements is minimum. Figure 5.39 gives a closer look at the Tx and Rx array arrangement.

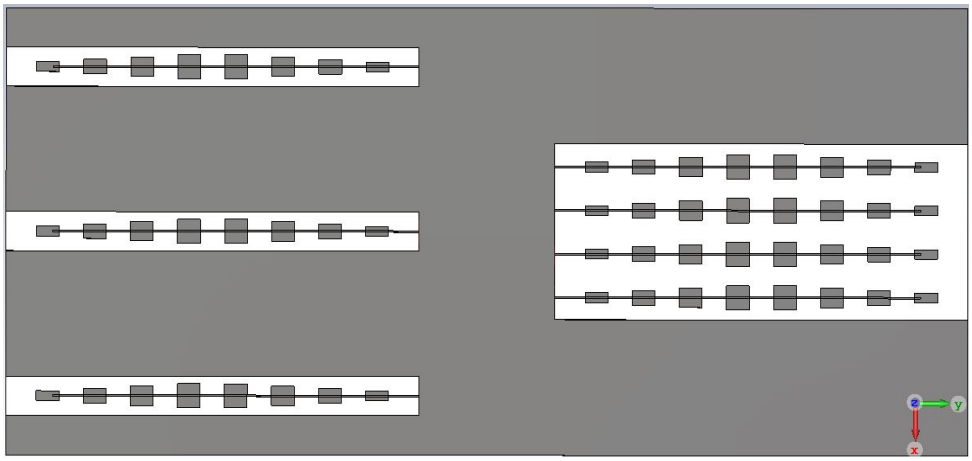

Figure 5.39: The Uniform Tx and Rx array arrangement

5.4.2. PERFORMANCE

Using the arrangement in figure 5.39, a scenario of a single target at 1 meters in the background of 5 interferes is simulated. The target is at angle of 10° and the 5 interference sources are positioned at 7°,30°,40°,−30°,−10° at a distance of 1m from the radar. An aluminum corner reflector is used as the target. The corner reflector is used because of having strong back scattering capabilities. The corner reflector is constructed by aligned three aluminum sheets of side lengths of 10mm and thickness of 0.02mm at right angles. The corner reflector is placed at 1m from the radar and at an angular position of 10°. A field probe is placed at the radar to measure the reflected target signal and interfering signals incident on the Rx array. Figure 5.42 shows the simulation scenario and figure 5.43 shows the aluminum corner reflector.

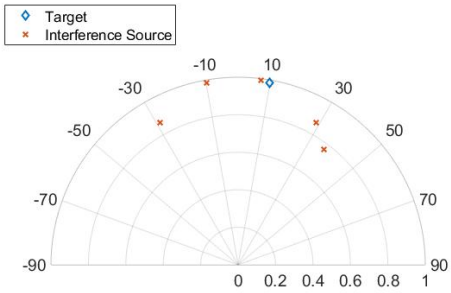

Figure 5.40: Simulation Scenario of one Target and Five interference sources

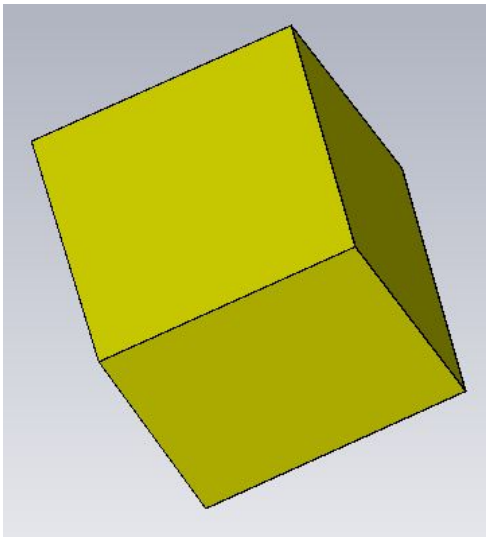

Figure 5.41: The Aluminum corner Reflector

For a MIMO system orthogonal Tx signals are required to from a virtual array. Orthogonality can be achieved by time-division multiplexing, frequency-division multiplexing and spatial coding. In this simulation the orthogonality is achieved by TDM (Time Division Multiplexing), which allows a single transmitter to transmit at a time. Each transmit element will generate four signals at the receiver, so for three transmitter elements 12 signals can be extracted from the receiver, these 12 signals form the virtual array data matrix, on which beamforming will be applied.

The signal is transmitted from the first Tx element, The signal travels 1m, reflects from the corner reflector and than travels 1m back to the radar. After suffering the path loss and the loss at the reflector, the target signal is incident on the Rx array. After travelling 1m the 5 interference signals are incident on the Rx array with a power of 3dBW.

The Rx array receives the target signal and five interference signals at the same time, so at the output port of the Rx array, we will see the combination of the target and interference signals. As the power of the incident interference signals is comparable to the power of the incident target signal, the combination of the target and the interference signals will cause the target information to be lost or corrupted, resulting in an inaccurate measurement. At the Rx output we will have 4 signals from the 4 Rx ports. Same is repeated for the other two Tx elements, and the 4 Rx signals for each Tx are than concatenated in one virtual array matrix. The beamforming from chapter 2 is applied on the virtual array data matrix to extract the target signal.

Table 5.1 shows the values SINR at the output of the beamformer for MATLAB and CST simulation for three cases when the power of the incoming target signal is 0,5 and 10dBW, while the power of the interference signals is 3dBW for the three cases. We can see that the improvement in output SINR for the non-uniform array for the CST simulation is close to the improvement for the MATLAB simulation. The degradation in the actual SINR value for the CST simulation is due to the fact that mutual coupling, losses in antenna and the dielectric are considered in the CST simulation, which will degrade the signal quality further.

Target Power	Interference Power	MATLAB		CST	
		Uniform	Non-Uniform	Uniform	Non-Uniform
0dBW	3dBW	3.987dB	5.65dB	2.7581dB	4.2520dB
5dBW	3dBW	9.085dB	10.58dB	7.6612dB	9.1573dB
10dBW	3dBW	13.93dB	15.59dB	12.5155dB	14.1863dB

Table 5.1: Comparison of output SINRs for MATLAB and CST simulations

From table 5.1, we can see that the SINR for the non-uniform array for the three cases, for the MATLAB simulations improves by about 1.6dB where as the SINR for CST simulations improves by about 1.5dB, hence the CST simulation verifies that the non-uniform MIMO antenna will perform better compared to the uniform MIMO antenna.

5.5. CONCLUSION

In this chapter the Results of chapter 4 are verified, by simulating the antenna arrangements from chapter 4 in CST using an antenna element designed for automotive applications. As a broadside radiation is required for automotive applications, a patch antenna is the best choice for it, but the broad beam of the patch antenna in the elevation plane indicates that a simple patch is not enough. To reduce the width of the elevation beam, the aperture of the patch antenna in the elevation (horizontal) plane is increased by connecting 8 patches in a column via a microstrip line. Furthermore to reduce the sidelobe level of the elevation beam the widths of the 8 patches are varied. By varying the widths, the sidelobe level in the elevation plane is reduced by 5.4dB.

The designed patch column is used as a single antenna element and by positioning the antenna element in accordance with the Tx and Rx array design proposed in chapter 4, the Tx and Rx arrays are constructed. The effect of mutual coupling is studied. The coupling effect on the elements of the non-uniform array will be lower due to increased spacing between elements compared to the uniformly spaced elements.

The performance of the modelled MIMO antenna system is checked for a single target surrounded by 5 interference sources. The power of the incoming target signal is varied from 0dBW to 10dBW, while the power of each of the incoming interference signals is kept constant at 3dBW. For all three cases of different target signal power, the MATLAB simulation shows an improvement of SINR of 1.6dB in favour of the non-uniform array, while the CST simulation shows an improvement of SINR of 1.5dB in favour of the non-uniform array, hence the CST simulation verifies the validity of the proposed non-uniform MIMO array design.

6

CONCLUSIONS AND FUTURE WORK

6.1. CONCLUSIONS

In this thesis, impact of spatial filtering by means of MIMO array on interference suppression in MIMO radar has been studied both at the signal processing (beamforming) level and at the antenna array level. An adaptive beamformer is derived, as the conventional beamformer is ineffective in the presence of high power interference signals. To compute the weights for the adaptive beamformer the covariance matrix for interference plus noise is required which is not available in practice, so the method of SMI is employed to estimate the sample covariance matrix. For this thesis a target free sample covariance is estimated. The goal of the derived adaptive beamformer is to minimize the interference plus noise power while maintaining a distortion less response in the direction of the target.

Regarding antenna array optimization, two distinctive design techniques to design the Tx and Rx array for a MIMO radar are analyzed. For the first technique a thinning method is proposed, which removes antenna elements from a large array of size K to form a non-uniform array of low sidelobes of size N while $K < N$. The thinning strategy is used to design the virtual array of the MIMO radar. A non-uniform MIMO virtual array of 12 elements is designed by removing the elements from a uniform array of 16 elements, which yields one design. The pattern of the final design is factorized to obtain the Tx and Rx patterns and antenna arrangements. The second technique employs the method of convex optimization to synthesize a non-uniform MIMO virtual array with low sidelobes when the main beam is scanned at various angles. The synthesized array is then factorized to obtain the non-uniform Tx and Rx arrays. Using the optimization problem Non-uniform Tx and Rx arrays are designed for two non-uniform MIMO virtual arrays, a virtual array of 12 elements and 24 elements. The factorization of the virtual array patterns yields multiple designs but as all the designs are factors of the same array, they will perform the same, so any of the Tx and Rx designs can be chosen.

The performance of the various designs obtained by the two design techniques is compared with the uniformly spaced linear MIMO array, for 500 realizations of a single

target surrounded by 5 interference sources at random positions. The average SINR for the 500 realizations at the output of the adaptive beamformer is used to decide which topology works the best.

The 12 element non-uniform array obtained via the thinning strategy improves the average SINR by 2.75dB for 2° separation, 2.45dB for 5° separation and 1.58dB for 10° separation of the target and the closest interference source. The 12 element non-uniform array via the multi beam optimization technique improves the average SINR by 3.35dB for 2° separation, 3.09dB for 5° separation and 2.13dB for 10° separation of the target and the closest interference source. The higher value of SINR for array via the multi beam optimization is due to lower sidelobes for the optimized array compared to the thinned array. The 24 element non-uniform array via the multi beam optimization technique improves the average SINR by 2.29dB for 2° separation, 1.69dB for 5° separation and 1dB for 10° separation of the target and the closest interference source.

From theses results we can conclude that the new designed topologies result up to 3.5dB improvement of the SINR in comparison to the currently used topologies. And the 3.5dB improvement of the SINR points to the fact that by just moving the antenna elements the radar will be able to detect objects twice as far with the same transmit power compared to the currently used topologies.

CST MS design environment is used to design and model a prototype for the designed topologies. A patch column with varying patch widths is used as a single antenna element to be used in the TX and Rx arrays. The prototype MIMO antenna system has lower mutual coupling between the elements, as the elements in the arrays are more spaced apart in comparison to the uniformly spaced arrays. The designed prototype is verified by simulating a scenario of a single target surrounded by five interference sources. The power of the signal incident on the Rx array is varied from 0dBW to 10dBW, while the power of each of the interference signals is fixed to 3dBW. The prototype model, based on the designed topologies discussed in this thesis, outperforms its uniformly spaced counterpart by increasing the output SINR by 1.5dB, which is close to the improvement in the output SINR of 1.6dB for the MATLAB simulations for the same simulation scenario.

6.2. FUTURE WORK

1. The performance of the designed topologies can be continually investigated for further processing algorithms such as the algorithms for angle of arrival estimation used in conjunction with the beamforming algorithm.

2. The radar model simulated in CST does not take into account the effects of moving target and interference sources, thus we can try to find a more effective model that will be able to incorporate the motion of the radar along with the moving target and interference sources.

3. The design techniques discussed here can be extended to 2-Dimensional arrays to optimize the array in the elevation and azimuth planes.

REFERENCES

REFERENCES

[1] Schnabel, R., Hellinger, R., Steinbuch, D., Selinger, J., Klar, M. and Lucas, B, "Development of a mid range automotive radar sensor for future driver assistance systems". *International Journal of Microwave and Wireless Technologies*, 5(01), pp.15-23. 2013

[2] S. Sanka, "Radar to radar interference for 77GHz automotive radar", *repository.tudelft.nl*, 2018. [Online]. Available: https://repository.tudelft.nl/islandora/object/uuid:3A6f4231ff-49ce-4f46-944a-3c15f86c50b4. [Accessed: 25- Aug- 2018].

[3] J. Overdevest, "Interference in 79 GHz Phase-Coded Automotive Radar", *repository.tudelft.nl*, 2018. [Online]. Available: http://uuid:a22d5686-0d83-402b-94cc-4b49c2a63853. [Accessed: 25- Aug- 2018].

[4] Dai, X., Xu, J., Peng, Y. and Xia, X. "High Resolution Range Imaging and Sidelobe Suppression Based on FD-MIMO Radar". *Journal of Electronics and Information Technology*, 30(9), pp.2033-2037, 2011

[5] D. Rabideau and P. Parker, "Ubiquitous MIMO multifunction digital array radar", *Proc, 37th Asilomar Conf, Signals, Systems, and Computers*, vol. 1, pp. 1057-1064, 2003.

[6] C. Chen and P. Vaidyanathan, "MIMO Radar Space–Time Adaptive Processing Using Prolate Spheroidal Wave Functions", *IEEE Transactions on Signal Processing*, vol. 56, no. 2, pp. 623-635, 2008.

[7] I. Bekkerman, J. Tabrikian. “Target Detection and Localization Using MIMO Radars and Sonars”, *IEEE Trans. Signal Process.*, 54, pp. 3873-3883, 2006.

[8] Jian Li, P. Stoica. “MIMO Radar with Colocated Antennas”, *IEEE Signal Process.* Mag., 24, pp. 106-114, 2007.

[9] A. Hassanien and S. Vorobyov, "Phased-MIMO Radar: A Tradeoff Between Phased-Array and MIMO Radars", *IEEE Transactions on Signal Processing*, vol. 58, no. 6, pp. 3137-3151, 2010.

[10] Rocca, P., Haupt, R. and Massa, A, "Interference Suppression in Uniform Linear Arrays Through a Dynamic Thinning Strategy". *IEEE Transactions on Antennas and Propagation*, 59(12), pp.4525-4533, 2011

[11] Jian Dong, Qingxia Li and Wei Guo, "A Combinatorial Method for Antenna Array Design in Minimum Redundancy MIMO Radars". *IEEE Antennas and Wireless Propagation Letters*, 8, pp.1150-1153, 2009

[12] Chun-Yang Chen, P. P. Vaidyanathan. “Minimum redundancy MIMO radars”, *IEEE International Symposium on Circuits and Systems*, pp. 45-48, 2008.

[13] D. G. Kurup, M. Himdi and A. Rydberg, “Synthesis of uniform amplitude unequally spaced antenna arrays using the differential evolution algorithm,” *IEEE Trans. Antennas Propag.*, vol. 51, no. 9, pp. 2210-2217, Sep. 2003.

[14] K. Chen, Z. He and C. Han, “A modified real GA for the sparse linear array synthesis with multiple constraints,” *IEEE Trans. Antennas Propag.*,vol. 54, no. 7, pp. 2169-2173, Jul. 2006.

[15] N. Jin and Y. Rahmat-Samii, “Advances in Particle Swarm Optimization for Antenna Designs: Real-Number, Binary, Single-Objective and Multiobjective Implementations,” *IEEE Trans. Antennas Propag.*, vol. 55, no.3, pp. 556-567, Mar. 2007.

[16] H. Oraizi and M. Fallahpour, “Nonuniformly spaced linear array design for the specified beamwidth/sidelobe level or specified directivity/sidelobe level with coupling considerations,” *Prog. Electromagn. Res. M*, vol. 4,pp. 185-209, 2008.

[17] Boeringer, D. and Werner, D. "Particle Swarm Optimization Versus Genetic Algorithms for Phased Array Synthesis". *IEEE Transactions on Antennas and Propagation*, 52(3), pp.771-779, 2004

[18] M. I. Skolnik, “Nonuniform arrays,” *in Antenna Theory*, R. E. Colin and F. J. Zucker, Eds. New York: McGraw-Hill, 1969, ch. 6, pt. 1.

[19] O. M. Bucci, M. D’Urso, T. Isernia, P. Angeletti and G. Toso, “Deterministic synthesis of uniform amplitude sparse arrays via new density taper techniques,” *IEEE Trans. Antennas Propag.*, vol. 58, no.6, pp. 1949-1958, Jun. 2010.

[20] M. C. Vigano and D. Caratelli, “Analytical synthesis technique for uniform-amplitude linear sparse arrays,” in *IEEE AP-S / URSI Symp.*, Toronto, Canada, Jul. 2010.

[21] A. F. Morabito, T. Isernia and L. Di Donato, “Optimal synthesis of phase-only reconfigurable linear sparse arrays having uniform-amplitude excitations,” *Prog. Electromagn. Res.*, vol. 124, pp. 405-423, 2012.

[22] H. Lebret and S. Boyd, “Antenna pattern synthesis via convex optimization,” *IEEE Trans. Signal Process.*, vol. 45, no. 3, pp. 526-531, Mar.1997.

[23] S. E. Nai, W. Ser, Z. L. Yu and H. Chen, “Beampattern synthesis for linear and planar arrays with antenna selection by convex optimization,” *IEEE Trans. Antennas Propag.*, vol. 58, no. 12, pp. 3923-3930, Dec. 2010.

[24] G. Prisco and M. D’Urso, “Maximally sparse arrays via sequential convex optimization,” *IEEE Antennas Wireless Propag. Lett.*, vol. 11,pp. 192-195, Feb. 2012.

[25] C. Bencivenni, M. V. Ivashina, R. Maaskant and J. Wettergren, “Design of maximally sparse antenna arrays in the presence of mutual coupling,” *IEEE Antennas Wireless Propag. Lett.*, vol. 14, pp. 159-162, Sep. 2014.

[26] C. Bencivenni, M. V. Ivashina, R. Maaskant and J. Wettergren, “Synthesis of maximally sparse arrays using compressive sensing and full-wave analysis for global earth coverage applications,” *IEEE Trans. Antennas Propag.*, vol. 64, no. 11, pp. 4872-4877, Jul. 2016.

[27] B. Fuchs, A. Skrivervik and J R. Mosig, “Synthesis of uniform amplitude focused beam arrays,” *IEEE Antennas Wireless Propag. Lett.*, vol. 11,pp.1178-1181, Oct. 2012.

[28] Y. Aslan, J. Puskely, A. Roederer and A. Yarovoy, "Synthesis of Multiple Beam Linear Arrays with Uniform Amplitudes", 2018.

[29] S. Mitra, K. Mondal, M. Tchobanou and G. Dolecek, "General polynomial factorization-based design of sparse periodic linear arrays", *IEEE Transactions on Ultrasonics, Ferroelectrics and Frequency Control*, vol. 57, no. 9, pp. 1952-1966, 2010.

[30] S. K. Mitra, *Digital Signal Processing: A Computer-Based Approach*, 3rd ed., New York, NY: McGraw-Hill, 2006.

[31] S. K. Mitra, M. K. Tchobanou, and M. I. Bryukhanov, “A general method for designing sparse antenna arrays,” *Proc. 17th European Conf. Circuit Theory and Design*, Cork, Ireland, Aug. 2005, vol. II, pp. 263–266.

[32] G. Kouemou, *Radar technology*. SL: Sciyo.com, 2010.